Quantum Monte Carlo method for the ground state of many-boson systems

Wirawan Purwanto* and Shiwei Zhang†
Department of Physics, The College of William and Mary, Williamsburg, Virginia 23187, USA
(Received 22 March 2004; published 9 November 2004)

We formulate a quantum Monte Carlo (QMC) method for calculating the ground state of many-boson systems. The method is based on a field-theoretical approach, and is closely related to existing fermion auxiliary-field QMC methods which are applied in several fields of physics. The ground-state projection is implemented as a branching random walk in the space of permanents consisting of identical single-particle orbitals. Any single-particle basis can be used, and the method is in principle exact. We illustrate this method with a trapped atomic boson gas, where the atoms interact via an attractive or repulsive contact two-body potential. We choose as the single-particle basis a real-space grid. We compare with exact results in small systems and arbitrarily sized systems of untrapped bosons with attractive interactions in one dimension, where analytical solutions exist. We also compare with the corresponding Gross-Pitaevskii (GP) mean-field calculations for trapped atoms, and discuss the close formal relation between our method and the GP approach. Our method provides a way to systematically improve upon GP while using the same framework, capturing interaction and correlation effects with a stochastic, coherent ensemble of noninteracting solutions. We discuss various algorithmic issues, including importance sampling and the back-propagation technique for computing observables, and illustrate them with numerical studies. We show results for systems with up to $N \sim 400$ bosons.

DOI: 10.1103/PhysRevE.70.056702 PACS number(s): 02.70.Ss, 03.75.Hh

I. INTRODUCTION

The study of many-body quantum systems has been a very challenging research field for many years. Computational methods have often been the way of choice to extract theoretical understanding on such systems. Most computational quantum-mechanical studies are based on simpler mean-field theories such as the Gross-Pitaevskii (GP) equation for bosons or the Kohn-Sham density-functional theory (DFT) for fermions. Despite their remarkable success, the treatment of particle interaction or correlation effects is only approximate within these approaches, and can lead to incorrect results, especially as the strength of particle interactions is increased. It is therefore necessary to develop alternative computational methods that can describe the effect of interaction more accurately and reliably.

In this paper, we present a quantum Monte Carlo (QMC) method to study the ground state of many-boson systems. The method is in principle exact aside from controllable statistical and discretization errors. Our interest in the development and use of this method was motivated by the realization of the Bose-Einstein condensation in ultracold atomic gases [1]. These are dilute gases consisting of interacting alkali-metal atoms. The atomic interaction is well described by a simple two-body potential, either attractive or repulsive, depending on the scattering length. For weakly interacting systems, the mean-field GP approach has, as expected, performed extremely well [2,3]. More recently, Feshbach resonances [4] have successfully been used as a powerful way to tune the strength of the interaction experimentally. This provides a source of rich physics, and increases the need for theoretical methods which can benchmark GP and provide an alternative where GP is inadequate.

Several QMC methods exist for calculating the properties of interacting many-body systems. The ground-state diffusion Monte Carlo [5] and the finite-temperature path-integral Monte Carlo (PIMC) [6] methods, which work in many-particle configuration space and in the first-quantized framework, have been successfully applied to a variety of boson and fermion systems. In the context of atomic gases, Krauth [7], Gruter *et al.* [8], and Holzmann and Krauth [9] have employed PIMC to study finite-temperature properties of trapped bosons with positive scattering lengths, modeling the two-body interactions by a hard-sphere potential. Glyde and co-workers have studied the ground state of trapped bosons, also by hard spheres [10,11]. Ulmke and Scalletar [12] did finite-temperature QMC calculations on quantum spin systems and the Bose-Hubbard model. In the latter calculation, a hard-core repulsive potential was assumed, which allowed a transformation of the problem into an *XXZ* spinlike problem that can be treated with a fermion QMC method.

Our method is based on the auxiliary-field quantum Monte Carlo (AFQMC) approach [13,14]. The AFQMC is a field-theoretical method, where many-body propagators resulting from two-body interactions are transformed, by use of auxiliary fields, into a many-dimensional integral over one-body propagators [15,16]. The many-dimensional integral is then computed using stochastic means. The AFQMC framework is appealing for several reasons. Working in second-quantization, it automatically imposes the proper particle-permutation symmetry or antisymmetry. It provides a many-body method with close formal relation to mean-field approaches, as we discuss later. In addition, it allows convenient calculation of the observables and correlation functions.

*Electronic address: wirawan@camelot.physics.wm.edu
†Electronic address: shiwei@physics.wm.edu

The AFQMC method has been widely employed to study fermion systems in condensed matter [17–21], nuclear physics [22,23], and lattice gauge theory. Essentially no work has been done using AFQMC for interacting boson systems, however. In this paper, we formulate a ground-state method for many-boson systems. We project the many-body boson ground state from an initial trial state $|\Psi_T\rangle$. Our choice of $|\Psi_T\rangle$ is a permanent consisting of N identical single-particle orbitals, which was first suggested in a model calculation by Sugiyama and Koonin [14]. The many-body ground state is projected from $|\Psi_T\rangle$ with open-ended, branching random walks to sample the auxiliary fields. We formulate an importance sampling scheme, which greatly improves the efficiency of the method and makes possible simulations of large systems. We also discuss in detail the back-propagation technique which allows convenient calculation of virtually any ground-state observables.

Our method retains all the advantages of AFQMC. It allows the use of any single-particle basis, which in this paper is chosen to be a real-space grid. As we discuss in Sec. VI, it provides a means for true many-body calculations in a framework which closely relates to the GP approach. The approach can be viewed as a stochastic collection of parallel GP-like calculations whose "coherent" linear combination gives the interaction and correlation effects.

In this paper, we present our QMC method for bosons and discuss its behavior and characteristics. We use a trapped atomic boson gas as our test system, where the atoms interact via an attractive or repulsive contact two-body potential. A sufficiently detailed description of the method is given to facilitate implementation. Compared to its fermionic counterpart, our method here is formally simpler. It therefore also offers opportunities to study algorithmic issues. Because of the intense interest in methods for treating correlated systems (fermions or bosons) and the relatively early development stage of this type of QMC method, a second purpose of the paper is to use the bosonic test ground to explore, discuss, and illustrate the generic features of ground-state QMC methods based on auxiliary fields. The majority of the applications in this paper will be to systems where exact results are available for benchmark. These include small systems, which can be diagonalized exactly, and the case of untrapped bosons with attractive interactions in one dimension, where analytical solutions exist. It is worth emphasizing that the method scales gracefully (similar to GP) and allows calculations for a large number (N) of bosons. We will show results for larger systems ($\sim$1000 sites and hundreds of particles) in one and three dimensions to illustrate this.

Our paper is organized as follows. In Sec. II, we establish some conventions and review the basic ground-state projection and auxiliary-field quantum Monte Carlo method. In Sec. III, we introduce our method for bosons, including the formulation of an importance-sampling scheme and the back-propagation technique for convenient calculation of virtually any ground-state observables. In Sec. IV, we describe the implementation of our method to study the ground state of a trapped Bose atomic gas, which we model by a Bose-Hubbard Hamiltonian with an external trapping potential. We also describe our implementation of the GP approach to study the same Hamiltonian. In Sec. V, we present our computational results from both QMC and GP. In Sec. VI, we discuss the relation between QMC and GP, comment on computing issues, and present our concluding remarks. Finally, in the Appendixes we provide additional technical details of the method.

II. BACKGROUND

A. Many-body Hamiltonian

We use the second-quantized formalism throughout this paper. We assume that an appropriate set of single-particle basis $\{|\chi_i\rangle\}$ has been chosen, in terms of which the wave functions will be expanded. For simplicity, we assume that the single-particle basis is orthonormal, although this is not required. The number of basis states is M. The operators $c_i^\dagger$ and c_i, respectively, are the usual creation and annihilation operators for the state $|\chi_i\rangle$. They satisfy the commutation relation $[c_i, c_j^\dagger]_- = \delta_{ij}$. This automatically imposes the symmetrization requirement of the many-body wave functions.

We limit our discussion to a quantum-mechanical, many-body system with two-body interactions. The Hamiltonian $\hat{H}$ has a general form of

$$\hat{H} = \hat{K} + \hat{V}, \tag{1}$$

where $\hat{K}$ is the sum total of all the one-body operators (the kinetic energy and external potential energy),

$$\hat{K} = \sum_{ij} K_{ij} c_i^\dagger c_j,$$

and $\hat{V}$ contains the two-body interactions,

$$\hat{V} = \sum_{ijkl} V_{ijkl} c_i^\dagger c_j^\dagger c_k c_l.$$

Our objective is to calculate the ground-state properties of such a system, which contains a fixed number of particles, N.

B. Ground-state projection

The ground-state wave function $|\Phi_0\rangle$ can be readily extracted from a given trial solution $|\Psi_T\rangle$ using the ground-state projection operator

$$\mathcal{P}_{\mathrm{gs}} \equiv e^{-\Delta\tau \hat{H}} e^{\Delta\tau E_T}, \tag{2}$$

where E_T is the best guess of the ground-state energy, provided that $|\Psi_T\rangle$ is not orthogonal to $|\Phi_0\rangle$. Applying the operator $\mathcal{P}_{\mathrm{gs}}$ repeatedly to $|\Psi_T\rangle$ would exponentially attenuate its excited-state components, leaving only the ground state,

$$(\mathcal{P}_{\rm gs})^n|\Psi_T\rangle \overset{n\to\infty}{\to} |\Phi_0\rangle, \tag{3a}$$

$$\mathcal{P}_{\rm gs}|\Phi_0\rangle \to |\Phi_0\rangle. \tag{3b}$$

Because of its resemblance to the real-time propagator, the operator $\mathcal{P}_{\rm gs}$ is also called the imaginary-time propagator. In ground-state QMC methods, $\mathcal{P}_{\rm gs}$ is evaluated by means of a Monte Carlo sampling, resulting in a stochastic representation of the ground-state wave function.

C. Basic auxiliary-field method

Two essential ingredients are needed in order to evaluate $\mathcal{P}_{\rm gs}$ within a reasonable computing time. The first is the Trotter-Suzuki approximation [24,25]. The propagator is broken up into a product of exponential operators, which becomes exact in the limit $\Delta\tau\to 0$. The second-order form of this approximation is

$$e^{-\Delta\tau(\hat{K}+\hat{V})} = e^{-(1/2)\Delta\tau\hat{K}}e^{-\Delta\tau\hat{V}}e^{-(1/2)\Delta\tau\hat{K}} + \mathcal{O}(\Delta\tau^3). \tag{4}$$

The second ingredient is the Hubbard-Stratonovich (HS) transformation [15,16], which allows us to reduce the two-body propagator to a multidimensional integral involving only one-body operators, using the following identity [26]:

$$e^{(1/2)\Delta\tau\hat{v}^2} = \frac{1}{\sqrt{2\pi}}\int_{-\infty}^{\infty} dx\, e^{-(1/2)x^2}e^{x\sqrt{\Delta\tau}\hat{v}}, \tag{5}$$

where $\hat{v}$ is a one-body operator: $\hat{v}\equiv\Sigma_{ij}v_{ij}c_i^\dagger c_j$. The hermiticity of $\hat{V}$ allows us to decompose it into a sum of the square of one-body operators $\{\hat{v}_i\}$ (see, e.g., Ref. [26]),

$$\hat{V} = -\frac{1}{2}\sum_i \hat{v}_i^2. \tag{6}$$

Because of this, we can always apply the HS transformation to a general two-body operator,

$$e^{-\Delta\tau\hat{V}} = \prod_i \int_{-\infty}^{\infty} dx_i \frac{e^{-(1/2)x_i^2}}{\sqrt{2\pi}} e^{x_i\sqrt{\Delta\tau}\hat{v}_i} + \mathcal{O}(\Delta\tau^2). \tag{7}$$

Applying these two procedures, we obtain an approximate expression of the ground-state projection operator,

$$\mathcal{P}_{\rm gs} = e^{\Delta\tau E_T}e^{-(1/2)\Delta\tau\hat{K}}\left\{\prod_i \int_{-\infty}^{\infty} dx_i p(x_i) e^{x_i\sqrt{\Delta\tau}\hat{v}_i}\right\} \times e^{-(1/2)\Delta\tau\hat{K}} + \mathcal{O}(\Delta\tau^2), \tag{8}$$

where $p(x)$ is the normalized Gaussian probability density function with unit standard deviation: $p(x) \equiv (1/\sqrt{2\pi})e^{-(1/2)x^2}$. This approach is applicable to both boson and fermion systems. It enables us to compute the exact ground state of a quantum many-body system. To reduce the systematic error from the finite time step $\Delta\tau$, the so-called "Trotter error," small time steps $\Delta\tau$ are necessary. Often, calculations are performed for several $\Delta\tau$ values. Then an extrapolation to $\Delta\tau\to 0$ is made to remove the Trotter error.

For convenience we define the following notations:

(a) $\vec{x}\equiv\{x_1,x_2,\ldots\}$: collection of all auxiliary fields.

(b) $p(\vec{x})\equiv\Pi_i p(x_i)$: a (normalized) multidimensional probability density function, which is the product of the one-dimensional probability density functions $p(x_i)$.

(c) $\hat{B}_v(\vec{x})$: a product of the exponential one-body operators arising from the auxiliary-field transformation. From Eq. (8), $\hat{B}_v(\vec{x})\equiv\Pi_i e^{x_i\sqrt{\Delta\tau}\hat{v}_i}$.

(d) $\hat{B}(\vec{x})$: the product of $\hat{B}_v(\vec{x})$ with all other one-body exponential operators that do not depend on the auxiliary fields $\vec{x}$, and all the necessary scalar prefactors. For the projector in Eq. (8), $\hat{B}(\vec{x})\equiv e^{\Delta\tau E_T}e^{-(1/2)\Delta\tau\hat{K}}\hat{B}_v(\vec{x})e^{-(1/2)\Delta\tau\hat{K}}$.

With these notations, $\mathcal{P}_{\rm gs}$ takes a generic form of a high-dimensional integral operator,

$$\mathcal{P}_{\rm gs} \approx \int d\vec{x}\, p(\vec{x})\hat{B}(\vec{x}). \tag{9}$$

D. Wave-function representation

We write our wave functions in terms of the basis functions $|\chi_i\rangle$. A single-particle wave function is written as

$$|\varphi\rangle = \sum_i \varphi_i|\chi_i\rangle = \sum_i \varphi_i c_i^\dagger|0\rangle \equiv \hat{\varphi}^\dagger|0\rangle. \tag{10}$$

A single-permanent, N-boson wave function is given by

$$|\phi\rangle = \hat{\phi}_1^\dagger\hat{\phi}_2^\dagger\cdots\hat{\phi}_N^\dagger|0\rangle. \tag{11}$$

In general, the exact ground-state wave function is a superposition of such permanents. Unlike the fermionic case, where the particles occupy mutually orthogonal orbitals, there is no such restriction on the orbitals here. We use this freedom in our method to have all the bosons occupy the same orbital in $|\phi\rangle$, which greatly simplifies the computation [14]. We will refer to this as the *identical orbital representation* (IOR). This representation eliminates the usual factorial computational complexity of permanents. The exponential of a one-body operator $\hat{A}$ [e.g., $\hat{B}(\vec{x})$] transforms a permanent into another permanent [27],

$$e^{\hat{A}}|\phi\rangle = |\phi'\rangle. \tag{12}$$

(In Appendix A, we include a brief summary of properties of wave functions in IOR.)

E. METROPOLIS AFQMC

Standard AFQMC calculations [14] employ METROPOLIS Monte Carlo algorithm to compute various ground-state observables,

$$\langle \hat{A} \rangle_{\rm gs} = \frac{\langle \Psi_T | \mathcal{P}_{\rm gs} \cdots \mathcal{P}_{\rm gs} \hat{A}\, \mathcal{P}_{\rm gs} \cdots \mathcal{P}_{\rm gs} | \Psi_T \rangle}{\langle \Psi_T | \mathcal{P}_{\rm gs} \cdots \mathcal{P}_{\rm gs} | \Psi_T \rangle}$$

$$= \frac{\int \mathcal{D}(\{\vec{x}_m, \vec{y}_n\}) P(\{\vec{x}_m, \vec{y}_n\}) \langle \Psi_T | \prod_m \hat{B}(\vec{x}_m) \hat{A} \prod_n \hat{B}(\vec{y}_n) | \Psi_T \rangle}{\int \mathcal{D}(\{\vec{x}_m, \vec{y}_n\}) P(\{\vec{x}_m, \vec{y}_n\}) \langle \Psi_T | \prod_m \hat{B}(\vec{x}_m) \prod_n \hat{B}(\vec{y}_n) | \Psi_T \rangle}$$

$$= \frac{\int \mathcal{D}(\{\vec{x}_m, \vec{y}_n\}) P(\{\vec{x}_m, \vec{y}_n\}) \langle \eta(\{\vec{x}_m\}) | \phi(\{\vec{y}_n\}) \frac{\langle \eta(\{\vec{x}_m\}) | \hat{A} | \phi(\{\vec{y}_n\}) \rangle}{\langle \eta(\{\vec{x}_m\}) | \phi(\{\vec{y}_n\}) \rangle}}{\int \mathcal{D}(\{\vec{x}_m, \vec{y}_n\}) P(\{\vec{x}_m, \vec{y}_n\}) \langle \eta(\{\vec{x}_m\}) | \phi(\{\vec{y}_n\}) \rangle}, \tag{13}$$

where

$$\mathcal{D}(\{\vec{x}_m, \vec{y}_n\}) \equiv \prod_m d\vec{x}_m \prod_n d\vec{y}_n,$$

$$P(\{\vec{x}_m, \vec{y}_n\}) \equiv \prod_m p(\vec{x}_m) \prod_n p(\vec{y}_n),$$

and in the last line we have introduced the shorthand

$$\langle \eta(\{\vec{x}_m\}) | \equiv \langle \Psi_T | \prod_m \hat{B}(\vec{x}_m),$$

$$|\phi(\{\vec{y}_n\})\rangle \equiv \prod_n \hat{B}(\vec{y}_n) | \Psi_T \rangle.$$

The METROPOLIS simulation is carried out by sampling the probability density function defined by the integrand in the denominator. Given the choice of Ψ_T in the identical-orbital representation, this readily applies to bosons, which is how the model calculation by Sugiyama and Koonin [14] was done. The total length of the imaginary time is predetermined by $\Delta\tau$ and the number of $\hat{B}$ operators in the product.

III. A GROUND STATE METHOD FOR BOSONS

In this paper, we formulate an approach for ground-state calculations of bosons with branching random walks. There are several advantages in implementing the Monte Carlo sampling as a random-walk process. It is a true ground-state formalism with open-ended random walks which allow projection to long enough imaginary times. The sampling process can be made much more efficient than in standard AFQMC, by virtue of importance sampling with Ψ_T to guide the random walks. It also leads to a universal approach for bosons and fermions, where it is necessary to use the random-walk formalism in order to implement a constraint to deal with the sign and complex-phase problems [19,21].

A key observation is that we can choose an IOR single-permanent wave function as the initial wave function $|\Psi_T\rangle$. At each imaginary time step $\tau \equiv n\,\Delta\tau$ in the projection in Eq. (3), the wave function is stochastically sampled by a collection of single-permanent wave functions $\{|\phi_{\rm i}^{(\tau)}\rangle\}$, where the index i (in upright roman letter) is different from the basis index *i*. From Eqs. (9) and (12), we see that, with each walker $|\phi_{\rm i}^{(0)}\rangle$ initialized to $|\Psi_T\rangle$ in IOR, the resulting projection will lead to a superposition of single-permanent wave functions, all of which are in IOR.

Each permanent evolves by the stochastic application of $\mathcal{P}_{\rm gs}$, as follows: we randomly sample $\vec{x}$ from the probability density function $p(\vec{x})$, then apply $\hat{B}(\vec{x})$ on $|\phi_{\rm i}^{(\tau)}\rangle$,

$$|\phi_{\rm i}^{(\tau+\Delta\tau)}\rangle \leftarrow \hat{B}(\vec{x}) |\phi_{\rm i}^{(\tau)}\rangle. \tag{14}$$

We will call these permanents *random walkers*. The collection of these random walkers at each imaginary time step is also referred to as *population*.

The population must first be equilibrated so that the ground-state distribution is reached. After equilibrium the ground state is given stochastically by the collection of permanents,

$$|\Phi_0\rangle \doteq \sum_{\rm i} |\phi_{\rm i}\rangle. \tag{15}$$

The random-walk process naturally causes the walker's orbitals to fluctuate. In order to increase sampling efficiency, we may associate a *weight* factor $w_{\rm i}$ to each walker $|\phi_{\rm i}\rangle$. For example, we can use the walker's amplitude as the weight factor,

$$w_{\rm i} \equiv \sqrt{\langle \phi_{\rm i} | \phi_{\rm i} \rangle}.$$

A better definition of the weight will be introduced later when we discuss importance sampling. We duplicate a walker when its weight exceeds a preset threshold. Conversely, walkers with small weights (lower than a predetermined limit) should be eliminated with the corresponding probability. In this way, the walkers will have roughly the same weight. This results in a branching random walk.

A. Measurement: "Brute force" and mixed estimators

The ground-state expectation value of an observable $\hat{A}$ is

$$\langle \hat{A} \rangle_{\rm gs} = \frac{\langle \Phi_0 | \hat{A} | \Phi_0 \rangle}{\langle \Phi_0 | \Phi_0 \rangle}. \tag{16}$$

In principle, we can use the same Monte Carlo samples as both $\langle \Phi_0 |$ and $|\Phi_0\rangle$. A "brute force" measurement on the population $\{|\phi_{\rm i}^{(\tau)}\rangle\}$ at imaginary time τ is given by

$$\langle \hat{A} \rangle_{\rm bf}^{(\tau)} \equiv \frac{\sum_{\rm ij} \langle \phi_{\rm j}^{(\tau)} | \hat{A} | \phi_{\rm i}^{(\tau)} \rangle}{\sum_{\rm ij} \langle \phi_{\rm j}^{(\tau)} | \phi_{\rm i}^{(\tau)} \rangle} \tag{17}$$

and the estimator $\langle \hat{A} \rangle_{\rm bf}$ is the average of such measurements. The "brute force" estimator is not useful in real-space-based QMC methods such as diffusion Monte Carlo, because the overlaps between different walkers would lead to δ functions. Here the walkers are nonorthogonal mean-field wave functions, and Eq. (17) is well defined in principle. The estimator is exact for all observables in the limit of large $N_{\rm wlkr}$. The ground-state energy estimated in this way is variational, namely, the computed energy lies higher than the exact value (outside of the statistical error bar) and converges to the exact value as $N_{\rm wlkr}$ is increased. In practice, however, the usefulness of the "brute force" estimator is limited to smaller systems. In general, it will have large variances. Reducing the variance is expensive because $\langle \hat{A} \rangle_{\rm bf}$ scales as $\mathcal{O}(N_{\rm wlkr}^2)$, where $N_{\rm wlkr}$ is the size of the population used to represent $|\Phi_0\rangle$.

The simplest approach to measuring the observables is the mixed estimator, i.e.,

$$\langle \hat{A} \rangle_{\rm mix} \equiv \frac{\langle \psi_T | \hat{A} | \Phi_0 \rangle}{\langle \psi_T | \Phi_0 \rangle}. \tag{18}$$

For example, to compute the ground-state energy, we can introduce the so-called local energy $E_L[\psi_T, \phi]$,

$$E_L[\psi_T, \phi] = \frac{\langle \psi_T | \hat{H} | \phi \rangle}{\langle \psi_T | \phi \rangle}. \tag{19}$$

The ground-state energy is obtained from the weighted sum of the local energies associated with each walker,

$$E_{\rm mix} = \frac{\sum_{\rm i} \langle \psi_T | \phi_{\rm i} \rangle E_L[\psi_T, \phi_{\rm i}]}{\sum_{\rm i} \langle \psi_T | \phi_{\rm i} \rangle}. \tag{20}$$

The local energy for each walker can be computed using the formula given in Appendix A.

The mixed estimator in Eq. (18) is exact only if the operator $\hat{A}$ commutes with the Hamiltonian. Otherwise, a systematic error arises. Nonetheless, the mixed estimator often gives an improvement over the purely variational estimator,

$$\langle \hat{A} \rangle_T \equiv \frac{\langle \Psi_T | \hat{A} | \Psi_T \rangle}{\langle \Psi_T | \Psi_T \rangle}. \tag{21}$$

Two formulas are often employed to correct for the systematic error,

$$\langle \hat{A} \rangle_{\rm extrap1} \equiv 2 \langle \hat{A} \rangle_{\rm mix} - \langle \hat{A} \rangle_T, \tag{22}$$

$$\langle \hat{A} \rangle_{\rm extrap2} \equiv \frac{\langle \hat{A} \rangle_{\rm mix}^2}{\langle \hat{A} \rangle_T}. \tag{23}$$

The second formula is useful for quantities such as density profile, which must be non-negative everywhere. These corrections are good only if $|\Psi_T\rangle$ does not differ significantly from $|\Phi_0\rangle$. In general, we need the back-propagation scheme to obtain the correct ground-state properties. We will describe this method after introducing importance sampling.

B. Importance sampling

In practice, the efficiency of the bare random walk described earlier is very low, because the random walks naively sample the Hilbert space, causing the weights of the walkers to fluctuate greatly. This results in large statistical noise. We formulate an importance sampling procedure [19,21]—using the information provided by the trial wave function $|\Psi_T\rangle$—to guide the random walk into the region where the expected contribution to the wave function is large.

1. Importance-sampled random walkers

An importance-sampled walker also consists of a permanent and a weight, although the weight will be redefined according to the projected overlap of the permanent with the trial wave function. The purpose is to define a random-walk process which will lead to a stochastic representation of the ground-state wave function in the form

$$|\Phi_0\rangle \doteq \sum_{\rm i} w_{\rm i} \frac{|\phi_{\rm i}\rangle}{\langle \Psi_T | \phi_{\rm i} \rangle}, \tag{24}$$

where $w_{\rm i}$ is the new weight of the walker. The overlap enters to redefine the weight factor such that walkers which have large overlap with $|\Psi_T\rangle$ will be considered "important" and will tend to be sampled more. Such walkers will also have greater contributions in the measured observables. Since the permanent now appears as a ratio $|\phi_{\rm i}\rangle / \langle \Psi_T | \phi_{\rm i} \rangle$, its normalization is no longer relevant and can be discarded, unlike in the unguided random walk. The only meaningful information in $|\phi_{\rm i}\rangle$ is its position in the permanent space.

2. Modified auxiliary-field transformation

Now we describe the random-walk process for the modified walkers. The goal is to modify $\mathcal{P}_{\rm gs}$ in Eq. (9) such that the random-walk process leads to random walkers with the characteristics described above in Eq. (24). The basic idea is the same as that in Ref. [19]. The main difference is that here we are dealing with bosons. In addition, the HS fields in Ref. [19] are discrete Ising-like, which allowed simplifications in the importance sampling, while here the auxiliary fields are continuous and thus a more general formalism will be developed. Our mathematical derivation here follows that of Ref. [21]. Up to now we have assumed that $\langle \Psi_T | \phi_{\rm i} \rangle$ is real and positive. There is therefore no additional subtlety with the meaning of importance sampling and the correct form of the

overlap to use, which Ref. [21] addressed in the context of fermionic calculations with general interactions.

To derive the importance-sampled propagator, we plug Eq. (24) into Eq. (3b). We will focus on the two-body propagator, which is evaluated stochastically and is therefore affected by importance sampling in a nontrivial way.

The modified propagator, $\tilde{\mathcal{P}}_{\rm gs}$, consists of two parts. The first is a rewriting of Eq. (5),

$$e^{(1/2)\Delta\tau\hat{v}^2} = \frac{1}{\sqrt{2\pi}}\int_{-\infty}^{\infty} dx\, e^{-(1/2)x^2} e^{\underline{x}x-(1/2)\underline{x}^2} e^{\sqrt{\Delta\tau}\,(x-\underline{x})\hat{v}}, \quad (25)$$

where we have added an arbitrary shift $\underline{x}$ to the auxiliary field x in the auxiliary-field operator. This is a change of variable in the integral on the right-hand side and does not alter the result of the integral. The new propagator $\tilde{\mathcal{P}}_{\rm gs}$ must preserve the representation of $|\Phi_0\rangle$ in the form of Eq. (24), which dictates that the walkers propagate in the following manner:

$$w_{\rm i}^{(\tau+\Delta\tau)}\frac{|\phi_{\rm i}^{(\tau+\Delta\tau)}\rangle}{\langle\Psi_T|\phi_{\rm i}^{(\tau+\Delta\tau)}\rangle} \leftarrow w_{\rm i}^{(\tau)}\frac{|\phi_{\rm i}^{(\tau)}\rangle}{\langle\Psi_T|\phi_{\rm i}^{(\tau)}\rangle}. \quad (26)$$

The second part of $\tilde{\mathcal{P}}_{\rm gs}$ is a result of this requirement. By bringing the term $\langle\Psi_T|\phi_{\rm i}^{(\tau+\Delta\tau)}\rangle$ in Eq. (26) to the right-hand side, we obtain an overlap ratio $\langle\Psi_T|\phi_{\rm i}^{(\tau+\Delta\tau)}\rangle/\langle\Psi_T|\phi_{\rm i}^{(\tau)}\rangle$. Combining the two parts gives an importance-sampled propagator of the form

$$\tilde{\mathcal{P}}_{\rm gs}[\phi] \approx \int d\vec{x}\, p(\vec{x}) W(\vec{x},\phi)\hat{B}(\vec{x}-\underline{\vec{x}}), \quad (27)$$

where

$$W(\vec{x},\phi) \equiv \frac{\langle\Psi_T|\hat{B}(\vec{x}-\underline{\vec{x}})|\phi\rangle}{\langle\Psi_T|\phi\rangle} e^{\underline{\vec{x}}\cdot\vec{x}-(1/2)\underline{\vec{x}}\cdot\underline{\vec{x}}} \quad (28)$$

is the aggregate of all the scalar prefactors in the modified propagator. This propagator takes $\{w_{\rm i}^{(\tau)}, |\phi_{\rm i}^{(\tau)}\rangle\}$ and advances the population to $\{w_{\rm i}^{(\tau+\Delta\tau)}, |\phi_{\rm i}^{(\tau+\Delta\tau)}\rangle\}$, both of which represent $|\Phi_0\rangle$ in the form of Eq. (24).

Monte Carlo sampling of the new propagator $\tilde{\mathcal{P}}_{\rm gs}$ is similar to the one without importance samping. We sample $\vec{x}$ from a normal Gaussian distribution, and apply the operator $\hat{B}(\vec{x}-\underline{\vec{x}})$ to the current walker $|\phi_{\rm i}^{(\tau)}\rangle$. But now we accumulate an extra multiplicative weight factor $W(\vec{x},\phi_{\rm i}^{(\tau)})$ every time we apply Eq. (27),

$$|\phi_{\rm i}^{(\tau+\Delta\tau)}\rangle \leftarrow \hat{B}(\vec{x}-\underline{\vec{x}})|\phi_{\rm i}^{(\tau)}\rangle, \quad (29a)$$

$$w_{\rm i}^{(\tau+\Delta\tau)} \leftarrow W(\vec{x},\phi_{\rm i}^{(\tau)}) w_{\rm i}^{(\tau)}. \quad (29b)$$

Here we use the customary notation of vector dot product, e.g., $\underline{\vec{x}}\cdot\vec{x} \equiv \Sigma_i \underline{x}_i x_i$. Note that the weight factor $W(\vec{x},\phi_{\rm i}^{(\tau)})$ depends on $|\Psi_T\rangle$ and both the current $(\phi_{\rm i}^{(\tau)})$ and future $(\phi_{\rm i}^{(\tau+\Delta\tau)})$ walker positions.

3. The optimal choice for auxiliary-field shift $\underline{\vec{x}}$

The optimal importance sampling is achieved when each random walker contributes equally to the estimator. We therefore choose $\underline{\vec{x}}$ to minimize the fluctuation in the weight factor $w_{\rm i}$. We do so by minimizing the fluctuation of $W(\vec{x},\phi)$ with respect to x_i at its average $(x_i=0)$,

$$\frac{\partial}{\partial x_i}\left[\frac{\langle\Psi_T|\hat{B}(\vec{x}-\underline{\vec{x}})|\phi_{\rm i}\rangle}{\langle\Psi_T|\phi_{\rm i}\rangle} e^{\underline{\vec{x}}\cdot\vec{x}-(1/2)\underline{\vec{x}}\cdot\underline{\vec{x}}}\right]\Bigg|_{x_i=0} = 0.$$

It is sufficient to expand the exponentials in terms of $\Delta\tau$ and require the term linear in x_i to vanish, since this is the leading term, containing $\sqrt{\Delta\tau}$. The others are vanishingly small as $\Delta\tau\to 0$. The best choice for $\underline{x}_i$ that satisfies this requirement is

$$\underline{x}_i = -\sqrt{\Delta\tau}\,\frac{\langle\Psi_T|\hat{v}_i|\phi_{\rm i}\rangle}{\langle\Psi_T|\phi_{\rm i}\rangle} \equiv -\sqrt{\Delta\tau}\,\overline{v_i}. \quad (30)$$

This choice depends on the current walker position as well as $|\Psi_T\rangle$, which is to be expected, since the objective for the shift is to guide the random walk toward the region where $\langle\Psi_T|\phi_{\rm i}^{(\tau)}\rangle$ is large. With $\underline{\vec{x}}$ determined, the algorithm for the random walk, as given in Eq. (29), is now completely specified.

4. Local energy approximation

We can furthermore approximate the prefactor $W(\vec{x},\phi)$ in Eq. (28) to obtain a more elegant and compact expression. After rewriting the prefactor in the form of an exponential, expanding $\hat{B}(\vec{x}-\underline{\vec{x}})$ in terms of $\Delta\tau$, and ignoring terms higher than $\mathcal{O}(\Delta\tau)$ in the exponent, we obtain

$$\prod_i e^{(1/2)\Delta\tau(1-x_i^2)(\overline{v_i^2}-\overline{v_i}^2)} e^{(1/2)\Delta\tau\overline{v_i}^2}, \quad (31)$$

where

$$\overline{v_i^2} \equiv \frac{\langle\Psi_T|\hat{v}_i^2|\phi_{\rm i}\rangle}{\langle\Psi_T|\phi_{\rm i}\rangle}. \quad (32)$$

The product is over the basis index i, which should be distinguished from the walker index i. The latter is held fixed here. The first exponential in Eq. (31) can be ignored by noting that the average value of x_i^2 with respect to the Gaussian probability density function is unity. Setting $x_i^2\to 1$, i.e., evaluating the exponential at the mean value $\langle x_i^2\rangle$, is justified because $\overline{v_i^2}$ and $\overline{v_i}^2$ do not change drastically within one time step. We also note that $\frac{1}{2}\Sigma_i\overline{v_i^2} = -\langle\Psi_T|\hat{V}|\phi_{\rm i}\rangle/\langle\Psi_T|\phi_{\rm i}\rangle$, which is the mixed estimator of the potential energy with respect to the walker $|\phi_{\rm i}\rangle$. Combining this term with the similar contribution from the one-body propagator, we obtain a simple, approximate expression for Eq. (28),

$$W(\vec{x},\phi_{\rm i}) \approx e^{\Delta\tau(E_T - E_L[\Psi_T,\phi_{\rm i}])}, \quad (33)$$

where $E_L[\Psi_T,\phi_{\rm i}]$ is the local energy of $\phi_{\rm i}$ as defined in Eq. (19). Note that, contrary to Eq. (28), this form depends only on the current walker position and not the future, although in practice a symmetrized version can be used which replaces the local energy by the average of the two. For a good trial wave function, the local energy fluctuates less in the random walk. If the trial wave function is the exact ground-state

wave function, the local energy becomes a constant and the weight fluctuation is altogether eliminated.

The algorithm resulting from Eq. (33) is an *alternative* to Eq. (28). The two are identical and exact in the limit $\Delta\tau \to 0$, but can have different Trotter errors.

Our importance-sampling formalism has a formal similarity to that in the diffusion Monte Carlo (DMC) methods in real configuration space [28,29]. The local energy has a similar form and our shift to the auxiliary field can be formally related to the force bias in DMC. Subtle and important differences exist, however, in both the formalism and implementation of importance sampling in these methods [21].

C. Measurement: Back-propagation

With importance sampling, the mixed estimator in Eq. (18) is given by

$$\langle \hat{A} \rangle_{\mathrm{mix}} = \frac{\sum_{\mathrm{i}} w_{\mathrm{i}} \frac{\langle \Psi_T | \hat{A} | \phi_{\mathrm{i}} \rangle}{\langle \Psi_T | \phi_{\mathrm{i}} \rangle}}{\sum_{\mathrm{i}} w_{\mathrm{i}}}. \tag{34}$$

For example, the ground-state energy is

$$E_{\mathrm{mix}} = \frac{\sum_{\mathrm{i}} w_{\mathrm{i}} E_L[\psi_T, \phi_{\mathrm{i}}]}{\sum_{\mathrm{i}} w_{\mathrm{i}}}.$$

As mentioned earlier, the normalization of ϕ_{i} is irrelevant because ϕ_{i} only appears in ratios in any formula that defines the algorithm: Eqs. (24), (28), (30), (33), and (34). We can (and should) normalize the permanent as needed, and discard the resulting normalization factor.

The mixed estimator is often inadequate for computing observables whose operators do not commute with the Hamiltonian. For example, the condensate fraction in the attractive trapped Bose-Hubbard model is greater than 100% if the Green's function $\langle c_i^\dagger c_j \rangle$ is estimated using the mixed estimator. Therefore we have to propagate the wave functions on both the right- and the left-hand side of the operator,

$$\langle \hat{A} \rangle_{\mathrm{bp}} = \frac{\langle \Psi_T | e^{-\tau_{\mathrm{bp}} \hat{H}} \hat{A} | \Phi_0 \rangle}{\langle \Psi_T | e^{-\tau_{\mathrm{bp}} \hat{H}} | \Phi_0 \rangle}. \tag{35}$$

This estimator approaches the exact expectation value in Eq. (16) as τ_{bp} is increased. Zhang and co-workers proposed a back-propagation technique [19] that reuses the auxiliary-field "paths" from different segments of the simulation to obtain $\langle \Phi_0^{\mathrm{bp}}| \equiv \langle \Psi_T | e^{-\tau_{\mathrm{bp}} \hat{H}}$, while avoiding the N_{wlkr}^2 scaling of a brute-force evaluation with two separate populations for $\langle \Phi_0|$ and $|\Phi_0\rangle$. Here we give a more formal derivation and description of the technique, and implement it to bosons.

At imaginary time τ, the population is $\{|\phi_{\mathrm{i}}^{(\tau)}\rangle\}$, which represents $|\Phi_0\rangle$ in the form of Eq. (24). The propagator in the denominator in Eq. (35) can be viewed equivalently as operating on the left or the right. The latter is precisely the "normal" importance-sampled random walk from τ to the future time $\tau' \equiv \tau + \tau_{\mathrm{bp}}$, which consists of $n_{\mathrm{bp}} \equiv \tau_{\mathrm{bp}}/\Delta\tau$ steps. We first assume that there is no branching (birth/death of walkers) in the normal walk, i.e., the weights are fully multiplied according to Eq. (28). The random walk of each walker will generate a path in auxiliary-field space. For convenience we will denote the path-dependent operator $\hat{B}[\vec{x}_{\mathrm{i}}^{(\tau)} - \vec{\bar{x}}(\phi_{\mathrm{i}}^{(\tau)})]$ by $\hat{B}_{\mathrm{i}}^{(\tau)}$, and the weight factor $W(\vec{x}_{\mathrm{i}}^{(\tau)}, \phi_{\mathrm{i}}^{(\tau)})$ by $W_{\mathrm{i}}^{(\tau)}$. Further, we will denote the time-ordered product $\hat{B}_{\mathrm{i}}^{(\tau'-\Delta\tau)} \cdots \hat{B}_{\mathrm{i}}^{(\tau+\Delta\tau)} \hat{B}_{\mathrm{i}}^{(\tau)}$ by $\hat{B}_{\mathrm{i}}^{(\tau':\tau)}$, and correspondingly the product of $W_{\mathrm{i}}^{(\tau)}$ by $W_{\mathrm{i}}^{(\tau':\tau)}$. Each path defines a product

$$\frac{1}{\langle \Psi_T | \phi_{\mathrm{i}}^{(\tau')} \rangle} W_{\mathrm{i}}^{(\tau':\tau)} \hat{B}_{\mathrm{i}}^{(\tau':\tau)} \langle \Psi_T | \phi_{\mathrm{i}}^{(\tau)} \rangle. \tag{36}$$

Collectively these products give a stochastic representation of $e^{-\tau_{\mathrm{bp}} \hat{H}}$.

Replacing the operator $e^{-\tau_{\mathrm{bp}} \hat{H}}$ in the numerator and denominator of Eq. (35) with Eq. (36), and using the expression for $|\Phi_0\rangle$ given by Eq. (24), we obtain

$$\langle \hat{A} \rangle_{\mathrm{bp}} = \frac{\sum_{\mathrm{i}} \left\langle \Psi_T \left| \frac{1}{\langle \Psi_T | \phi_{\mathrm{i}}^{(\tau')} \rangle} W_{\mathrm{i}}^{(\tau':\tau)} \hat{B}_{\mathrm{i}}^{(\tau':\tau)} \hat{A}\, w_{\mathrm{i}}^{(\tau)} \right| \phi_{\mathrm{i}}^{(\tau)} \right\rangle}{\sum_{\mathrm{i}} \left\langle \Psi_T \left| \frac{1}{\langle \Psi_T | \phi_{\mathrm{i}}^{(\tau')} \rangle} W_{\mathrm{i}}^{(\tau':\tau)} \hat{B}_{\mathrm{i}}^{(\tau':\tau)} w_{\mathrm{i}}^{(\tau)} \right| \phi_{\mathrm{i}}^{(\tau)} \right\rangle}. \tag{37}$$

Using the propagation relation in Eq. (29), we can show that

$$\hat{B}_{\mathrm{i}}^{(\tau':\tau)} W_{\mathrm{i}}^{(\tau':\tau)} w_{\mathrm{i}}^{(\tau)} |\phi_{\mathrm{i}}^{(\tau)}\rangle = w_{\mathrm{i}}^{(\tau')} |\phi_{\mathrm{i}}^{(\tau')}\rangle, \tag{38}$$

i.e., the denominator in Eq. (37) reduces to $\Sigma_{\mathrm{i}} w_{\mathrm{i}}^{(\tau')}$. This result is to be expected, and can also be seen by completing the n_{bp} steps of the "normal" random walk we discussed above. With importance sampling, the Monte Carlo estimate of the denominator is simply given by the weights at time τ'.

To simplify the numerator in Eq. (37), we associate a *back-propagated* wave function with each walker $|\phi_{\mathrm{i}}^{(\tau)}\rangle$,

$$|\eta_{\mathrm{i}}^{(\tau_{\mathrm{bp}})}\rangle \equiv [\hat{B}_{\mathrm{i}}^{(\tau+\tau_{\mathrm{bp}}:\tau)}]^\dagger |\Psi_T\rangle. \tag{39}$$

Note that each of these η's originates from the trial wave function $|\Psi_T\rangle$, and is propagated by applying the $\hat{B}$'s in *reverse* order, as implied by the Hermitian conjugation. We may then write Eq. (37) in the following form:

$$\langle \hat{A} \rangle_{\mathrm{bp}} = \frac{\sum_{\mathrm{i}} w_{\mathrm{i}}^{(\tau')} \frac{\langle \eta_{\mathrm{i}}^{(\tau_{\mathrm{bp}})} | \hat{A} | \phi_{\mathrm{i}}^{(\tau)} \rangle}{\langle \eta_{\mathrm{i}}^{(\tau_{\mathrm{bp}})} | \phi_{\mathrm{i}}^{(\tau)} \rangle}}{\sum_{\mathrm{i}} w_{\mathrm{i}}^{(\tau')}}. \tag{40}$$

The estimators in Eqs. (35) and (40) parallel that of the standard AFQMC estimator in Eq. (13). The $|\phi\rangle$'s and $\langle \eta|$'s have similar meanings. The only difference lies in how the paths are generated. Here an open-ended random walk is used to advance an ensemble of paths from τ to τ', which

result in fluctuating weights that represent the path distribution. In standard AFQMC, a fixed length path (corresponding to $\tau_{bp}+\tau_{eq}$, with τ_{eq} being the minimum time for equilibriation or, failing that, the maximum time that can be managed by the calculation) is moved about by the METROPOLIS algorithm, which eliminates branching by the acceptance/rejection step. In other words, the estimators in Eq. (13) and (40) are the same except for the weights.

Equation (40) defines an algorithm for obtaining an estimate of $\langle\hat{A}\rangle_{bp}$ via the following steps: (i) A population is recorded as $\{|\phi_i^{(\tau)}\rangle\}$; (ii) as the random walk continues, the path history is kept for a time interval τ_{bp}; (iii) the population $\{|\eta_i^{(\tau_{bp})}\rangle\}$ is then generated by back-propagation using Eq. (39); (iv) this population is matched in a one-to-one manner to $\{|\phi_i^{(\tau)}\rangle\}$, weighted by the weight *at the later time*, $w_i^{(\tau')}$, and the estimator is formed.

In the back-propagation the propagators are, as shown in Eq. (39), identical to those in the forward direction, but in reverse order in imaginary time. As in the normal walk, the normalization of $|\eta_i^{(\tau_{bp})}\rangle$ does not enter in the estimator. Similar to the mixed estimator, this procedure can be repeated periodically to improve statistics. Evidently this estimator is exact in the limit of large τ_{bp}.

We have assumed that there is no branching within the interval τ_{bp}. In practice, a population control scheme is often used which causes the birth/death of walkers. This does not affect the derivation above or the basic algorithm. The effect on the implementation is that a list of ancestry links must be kept for the forward steps, which indicates the parent of each walker at each step in the imaginary-time duration τ_{bp}. As a result of branching, two or more $\langle\eta|$'s may share the same segment of the paths in their "past" and the same parent $|\phi_i^{(\tau)}\rangle$. The estimator remains exact for large τ_{bp}. Branching or weight fluctuation does have a more serious practical implication, however. As τ_{bp} is increased, more and more $\langle\eta|$'s will be traced back to the same parent $|\phi_i^{(\tau)}\rangle$. Or equivalently, fewer and fewer permanents in the set $\{|\phi_i^{(\tau)}\rangle\}$ will contribute to the estimator. This results in a loss of efficiency or an increase in variance. Better importance sampling will help improve the situation, often greatly, by reducing fluctuations in weights, although the problem will always occur at large enough τ_{bp}. In our applications to date we have rarely encountered the problem and find that the computed observables converge quite rapidly (see Sec. V for illustrative results).

IV. TRAPPED BOSON GAS: MODEL AND IMPLEMENTATIONS OF QMC AND GP METHODS

In this section, we discuss the model we use to describe a single-species, Bose atomic gas with pairwise contact interaction, confined in a harmonic trap in one or three dimensions. We then describe the implementations of both our QMC method and the standard mean-field GP approach to study this model. Numerical results will be presented in Sec. V.

A. Model

We use an effective potential characterized by the low-energy atom-atom scattering length, a_s. The two-body interaction takes a simple form

$$U(\mathbf{r}_1-\mathbf{r}_2)=\frac{4\pi a_s\hbar^2}{m}\delta(\mathbf{r}_1-\mathbf{r}_2). \tag{41}$$

For this effective potential to be valid, several assumptions are made; for example, the dominant effect is from *s*-wave scattering, and $|a_s|$ is much smaller than the average interparticle spacing. For more details, we refer the reader to Ref. [3]. In the alkali-metal gases these conditions are in general well met, and the model potential can be expected to give quantitative information, although care must be taken to validate the conditions.

The real-space Hamiltonian of trapped bosons in d dimensions is

$$\hat{H}=\int d^3\mathbf{r}\hat{\psi}^\dagger(\mathbf{r})\left(-\frac{\hbar^2}{2m}\nabla_{\mathbf{r}}^2+\frac{1}{2}m\omega_0^2r^2\right)\hat{\psi}(\mathbf{r})+\frac{1}{2}\frac{4\pi a_s\hbar^2}{m}\int d^3\mathbf{r}_1\int d^3\mathbf{r}_2\hat{\psi}^\dagger(\mathbf{r}_1)\hat{\psi}^\dagger(\mathbf{r}_2)\delta(\mathbf{r}_1-\mathbf{r}_2)\hat{\psi}(\mathbf{r}_2)\hat{\psi}(\mathbf{r}_1). \tag{42}$$

The one-body Hamiltonian $\hat{K}$ consists of the kinetic energy and the (external) confinement potential. The interaction Hamiltonian $\hat{V}$ is the sum of all the two-body potentials. The characteristic trap frequency is ω_0, which is related to the so-called oscillator length scale by $a_{ho}=\sqrt{\hbar/m\omega_0}$.

We introduce a real-space lattice, with a linear dimension of L, in a simulation cell of volume $(2r_b)^d$. The lattice spacing is therefore $\varsigma=2r_b/L$. Further, we will consider only a spherically symmetric trap here for simplicity. We truncate the simulation cell accordingly and assume that the wave function is negligible outside the maximum sphere enclosed by the cell.

The discretized Hamiltonian corresponding to Eq. (42) is

$$\hat{H}=\sum_i\left\{-t\left[\sum_{j\in \mathrm{NN}(i)}c_i^\dagger c_j-2dc_i^\dagger c_i\right]+\tfrac{1}{2}\kappa|\tilde{\mathbf{r}}_i-\tilde{\mathbf{r}}_0|^2c_i^\dagger c_i\right\}+\tfrac{1}{2}U\sum_i(c_i^\dagger c_i c_i^\dagger c_i-c_i^\dagger c_i), \tag{43}$$

where $c_i^\dagger$ and c_i are the usual creation and annihilation operators at site i. The Hubbard parameters t, U, and κ are related to the real, physical parameters as follows:

$$t = \frac{1}{2\varsigma^2}, \tag{44a}$$

$$U = \frac{4\pi a_s}{\varsigma^d}, \tag{44b}$$

$$\kappa = \frac{\varsigma^2}{a_{\mathrm{ho}}^4}, \tag{44c}$$

where for simplicity we have set $\hbar = m = 1$. The lattice coordinate $\tilde{\mathbf{r}}_i$ is related to the real coordinate by $\tilde{\mathbf{r}}_i = (L/2r_b)\mathbf{r}_i$, and $\tilde{\mathbf{r}}_0$ is the lattice coordinate of the trap's center. Note that a_s is the true scattering length only in three-dimensional systems. Nonetheless, we will retain the symbol a_s in Eq. (44b) as a convenient measure of the interaction strength in any dimension.

In the discretized model, our resolution is limited by the lattice spacing. This is consistent with the conditions of validity of the model interaction in Eq. (41), as it in a sense "integrates out" the short-range dynamics. In this model, the lattice constant ς must be much smaller compared to the average interparticle spacing, but larger than the scattering length,

$$|a_s| \ll \varsigma \ll \rho^{-1/d}. \tag{45}$$

With a negative a_s, the particles tend to "lump" together due to the gain in the interaction energy. This is a situation where we especially have to be aware of the validity of the effective potential. As mentioned, we will do a consistency check at the end of the calculation to ensure that the occupancy of the lattice points is less than unity.

B. Implementation of QMC

Implementation of our QMC method for this model is straightforward. The number of basis M is equal to the number of lattice sites inside the truncated sphere of radius r_b. The two-body term in Eq. (43) is in the desired form of Eq. (6). With a negative U, the HS transformation in Eq. (7) leads to M auxiliary fields, with one-body propagators in the form of $\exp(\sqrt{\Delta\tau|U|}x_i\hat{n}_i)$, where $\hat{n}_i \equiv c_i^\dagger c_i$ is the density operator. Our trial wave function $|\Psi_T\rangle$ is the Gross-Pitaevskii (GP) wave function Φ_{GP}, which we describe in the next subsection.

We mention here a technical point in the implementation. The ground-state projection in our method involves the application of one-body propagator in the form of $e^{\hat{A}}$ on a single-permanent wave function $|\phi\rangle$. This usually translates into a matrix-vector multiplication in the computer program, which generally costs $\mathcal{O}(M^2)$. Often there are special properties of $\hat{A}$ that can be exploited to evaluate the one-body propagator more efficiently. In the Bose-Hubbard Hamiltonian, the only nondiagonal part of the Hamiltonian in real space is the kinetic operator in $\hat{K}$. We can separate it from the other one-body operators and apply the kinetic propagator in momentum space. Wave functions are quickly translated between these two representations using fast Fourier transforms (FFT). In this way, the actual application of $e^{-(1/2)\Delta\tau\hat{K}}$ involves only diagonal matrices; thus the overall cost for each $e^{-(1/2)\Delta\tau\hat{K}}$ operation is reduced to $\mathcal{O}(M \log M)$. We observe in our calculations that the additional Trotter error is much smaller than the error already introduced in the original breakup, Eq. (4).

C. Implementation of the Gross-Pitaevskii self-consistent equation

The GP wave function Φ_{GP} is the single-permanent wave function

$$\Phi_{\mathrm{GP}}(\mathbf{r}_1, \mathbf{r}_2, \ldots, \mathbf{r}_N) = \varphi(\mathbf{r}_1)\varphi(\mathbf{r}_2)\cdots\varphi(\mathbf{r}_N), \tag{46}$$

which minimizes the expectation value of the ground-state energy. Such a wave function satisfies the self-consistent Gross-Pitaevskii equation [30–32]

$$-\frac{\hbar^2}{2m}\nabla^2\varphi(\mathbf{r}) + \frac{1}{2}m\omega_0^2|\mathbf{r}-\mathbf{r}_0|^2\varphi(\mathbf{r}) + \frac{(N-1)}{N}\frac{4\pi a_s\hbar^2}{m}|\varphi(\mathbf{r})|^2\varphi(\mathbf{r}) = \mu\varphi(\mathbf{r}). \tag{47}$$

[We keep the prefactor $(N-1)/N$, since we will study both large and small values of N.]

To compare our QMC results to those of mean field, we carry out GP calculations on the same lattice systems. The discretized GP Hamiltonian in the second-quantized form is

$$\hat{H}_{\mathrm{GP}} = -t\sum_i\left(\sum_{j\in \mathrm{NN}(i)} c_i^\dagger c_j - 2dc_i^\dagger c_i\right) + \frac{1}{2}\kappa\sum_i|\tilde{\mathbf{r}}_i - \tilde{\mathbf{r}}_0|^2 c_i^\dagger c_i + \frac{N-1}{N}U\sum_i\left(\overline{n_i}c_i^\dagger c_i - \tfrac{1}{2}\overline{n_i}^2\right). \tag{48}$$

Here $\overline{n_i}$ is the expectation value of the density operator,

$$\overline{n_i} \equiv \frac{\langle\Phi_{\mathrm{GP}}|c_i^\dagger c_i|\Phi_{\mathrm{GP}}\rangle}{\langle\Phi_{\mathrm{GP}}|\Phi_{\mathrm{GP}}\rangle}. \tag{49}$$

We have implemented two methods for solving the GP equation. The *first* is the usual self-consistent iterative approach. We generate an initial density profile, $\overline{n_i}^{(0)}$, by solving the noninteracting Hamiltonian (with $U=0$). The density is fed back to construct the initial Hamiltonian $\hat{H}_{\mathrm{GP}}^{(0)}$ in Eq. (48). Direct diagonalization of this one-body Hamiltonian yields its ground state $|\Phi_{\mathrm{GP}}^{(1)}\rangle$. We thus obtain an updated density $\overline{n_i}^{(1)}$ and a better Hamiltonian $\hat{H}_{\mathrm{GP}}^{(1)}$. This procedure is iterated until the desired convergence criterion is satisfied. We choose our convergence condition to be

$$\frac{\int d\mathbf{r}|\varphi^{(t+1)}(\mathbf{r}) - \varphi^{(t)}(\mathbf{r})|}{\frac{1}{2}\int d\mathbf{r}|\varphi^{(t+1)}(\mathbf{r}) + \varphi^{(t)}(\mathbf{r})|} < \epsilon, \tag{50}$$

where ϵ is a small number (usually on the order of 10^{-13} for double precision numbers).

The *second* method we use to solve Eq. (48) avoids the diagonalization procedure. It is closely related to the QMC method, both computationally and formally (see Sec. VI). We use the ground-state projector $e^{-\Delta\tau\hat{H}_{\mathrm{GP}}}$,

$$(e^{-\Delta\tau\hat{H}_{\mathrm{GP}}})^n|\Psi^{(0)}\rangle \overset{n\to\infty}{\to} |\Phi_{\mathrm{GP}}\rangle. \tag{51}$$

The initial wave function is arbitrary and can be, for example, chosen again as the solution with $U=0$. The feedback mechanism through the density profile $\overline{n_i}$ remains the same. By using FFT for the kinetic propagator as described in Sec. IV B, a speed gain is obtained, especially for large systems. In practice, we have often found this method to be a simpler and faster alternative to the first method of diagonalization and iteration. Note that the scalar term $-\frac{1}{2}[(N-1)/N]U\Sigma_i\overline{n_i}^2$ does not affect the projection process, but with it $\hat{H}_{\mathrm{GP}}$ corresponds to the original many-body Hamiltonian in that $\langle\Phi_{\mathrm{GP}}|\hat{H}_{\mathrm{GP}}|\Phi_{\mathrm{GP}}\rangle=\langle\Phi_{\mathrm{GP}}|\hat{H}|\Phi_{\mathrm{GP}}\rangle$.

V. RESULTS

In this section, we present results from our QMC and GP calculations in one, two, and three dimensions. To validate our method and illustrate its behavior, the majority of the calculations will be on systems where exact results are available for benchmark. These include small lattices, which can be diagonalized exactly, and the case of attractive δ-function interactions in one dimension, where analytic solutions exist. For the purpose of presenting the method to facilitate implementation, some numerical results and comparisons are shown in detail to illustrate the behavior and characteristics of the method.

Most of the results we present here will be for attractive interactions, where the method is exact and is free of any phase problem [21] from complex propagators (see Sec. V C). Such systems therefore provide a clean testground for our method. In addition, with attractive interactions the condensate in 3D is believed to collapse beyond a critical interaction strength or number of particles. Mean-field calculations [33] estimate the collapse critical point to be about $Na_s/a_{\mathrm{ho}}=-0.575$. The exact behavior of the condensate near the critical point is, however, not completely clear, as many-body effects are expected to have an impact. At the end of this section, we will also show some preliminary results for larger systems with both attractive and repulsive interactions in 3D.

We measure the ground-state expectation values of the following quantities: the ground-state energy, kinetic energy $\langle\hat{T}\rangle$, external confining potential $\langle\hat{V}_{\mathrm{trap}}\rangle$, interaction energy $\langle\hat{V}_{2B}\rangle$, density profile $\langle\hat{n}_i\rangle$, and the condensate fraction (often abbreviated "cond. frac." in the tables and figures). The condensate fraction is defined as the largest eigenvalue of the diagonalized density matrix [3]. If we write the one-body Green's-function matrix $\langle c_i^\dagger c_j\rangle$ in terms of its eigenvalues $\{n_\alpha\}$ and eigenvectors $\{\chi_\alpha(i)\}$,

$$\langle c_i^\dagger c_j\rangle = \sum_\alpha n_\alpha \chi_\alpha^\dagger(i)\chi_\alpha(j),$$

then the largest eigenvalue divided by the total number of particles gives the condensate fraction.

TABLE I. Comparison of QMC calculation against exact diagonalization (ED) and the Gross-Pitaveskii (GP) method. The system has 13 sites, 5 particles, $t=2.676, U=-1.538, \kappa=0.3503$. In the QMC calculation, we use $\Delta\tau=0.01$, $\tau_{\mathrm{bp}}=4.0$, and the GP solution as the trial wave function.

Type	ground-state energy	$\langle\hat{T}\rangle$	$\langle\hat{V}_{\mathrm{trap}}\rangle$	$\langle\hat{V}_{2B}\rangle$	Cond. frac.
ED	−1.009	4.278	0.8427	−6.129	95.59%
QMC	−1.008(2)	4.279(3)	0.8423(5)	−6.129(2)	95.59%
GP	−0.493	3.919	0.7504	−5.162	100%

A. Comparison with exact diagonalization: $a_s<0$

The many-body Hamiltonian (43) can be diagonalized exactly for small systems to benchmark our QMC calculation. We compare our QMC results with exact diagonalization for a one-dimensional lattice of 13 sites, and study its behavior for different values of the interaction strength a_s and number of particles N.

The first system we study has five bosons, with $t=2.676, U=-1.538$, and $\kappa=0.3503$. These values were derived from the physical parameters $a_{\mathrm{ho}}=8546$ Å and $a_s=-5.292\times10^{-6}$ Å^{-1}. (Recall that, by our definition, a_s in 1D does not have the dimension of length, and is not the scattering length itself.) For all systems in this section and in Sec. V C, we multiplied t, U, and κ by a factor of 10^8 Å^2 to make them dimensionless and close to unity. Our energies are therefore dimensionless. Table I shows the comparison of the quantities computed using three methods: QMC, GP, and exact diagonalization (ED). The statistical uncertainty of QMC results is presented in parentheses. We see that the agreement between QMC and ED is excellent. GP makes significant errors here because of the sizable interaction strength as well as the small number of particles.

To illustrate the convergence in imaginary time step $\Delta\tau$, we show in Fig. 1 the total energy and the average trap energy $\langle\hat{V}_{\mathrm{trap}}\rangle$. The former can be obtained exactly from the mixed estimator while the latter requires back-propagation. To show the Trotter error, we have deliberately done the calculations up to rather large $\Delta\tau$ values. We see that both quantities converge to the exact results as $\Delta\tau\to0$.

To illustrate the convergence of observables in back-propagation length, we show in Fig. 2 the various observables computed by QMC as a function of τ_{bp}. Separate calculations were done for different values of τ_{bp}. For all calculations, a small $\Delta\tau$ value of 0.01 was used. We see that, for observables that do not commute with $\hat{H}$, the mixed estimates ($\tau_{\mathrm{bp}}=0$) are indeed quite biased. The linear extrapolation in Eq. (22) with the variational (GP) estimate still leaves a significant error in most cases. In fact, for the kinetic

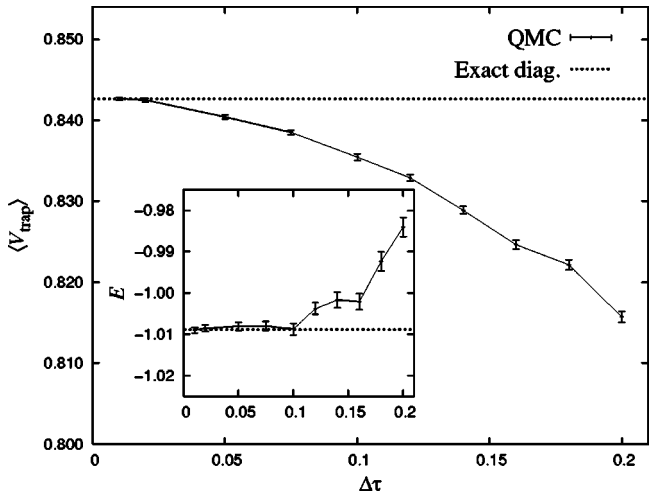

FIG. 1. Convergence of QMC observables with $\Delta\tau$. The main graph shows the trap energy $\langle \hat{V}_{trap} \rangle$, while the inset shows the total energy, E. The energies and $\Delta\tau$ are dimensionless, as explained in the text. The system has the same parameters as in Table I. Lines connecting QMC data are to aid the eye.

energy it gives a worse estimate. With back-propagation, all quantities converge to the exact results rather quickly, by $\tau_{bp} \sim 2$. (The total energy $\langle H \rangle$ is of course exact for any τ_{bp}, including $\tau_{bp}=0$.) The energy expectation values show that this is a system with significant interaction effects. Alkali-metal systems at the experimental parameters often have weaker interaction strengths, and the convergence rate is expected to be even faster.

Our QMC method is exact and therefore independent of the trial wave function Ψ_T, except for convergence rate and statistical errors. In Fig. 3, we show QMC results obtained using two different Ψ_T's, namely the noninteracting solution and the GP wave function. The convergence of condensate fraction and trap energy are shown versus back-propagation

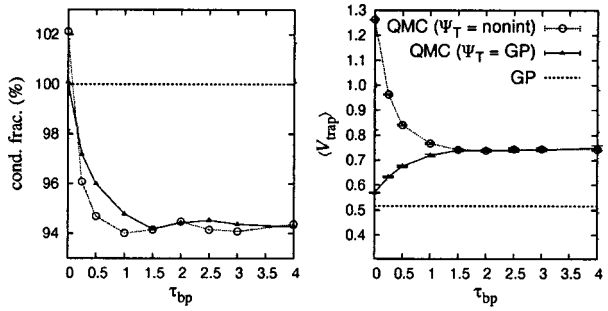

FIG. 3. Independence of QMC results on trial wave functions ("GP" for Gross-Pitaevskii, "nonint" for noninteracting solution). The system is the same as in Table I, except that here we use six particles. The horizontal axes are the back-propagation length.

time τ_{bp} for a system of six particles on 13 sites. The calculations lead to the same results. The quality of Ψ_T, however, does affect the variances of the observables and their convergence rates with τ_{bp}. For example, the noninteracting wave function, which disregards the two-body interaction, is more extended (in its density profile) than GP. Its mixed estimator is therefore worse than that with the GP trial wave function. The mixed estimator for the ground-state energy is exact in both, but the variance is slightly larger with the former.

We now show results for different systems with N from two to nine bosons and varying interaction strengths. We note that if we keep the product $(N-1)U$ constant, the Gross-Pitaevskii equation predicts the same *per-particle* energies and densities. For brevity, we shall refer to the curve in which $(N-1)U$ is constant as the *GP isoline*. Deviation from the GP isoline is therefore an indication of the effect of many-body correlations. In order to show results on multiple systems at the same time, we will scan GP isolines. Figure 4 shows the QMC and GP results as a function of the number of particles. In the GP calculations, the per-particle quantities are constants. The QMC results, on the other hand, capture

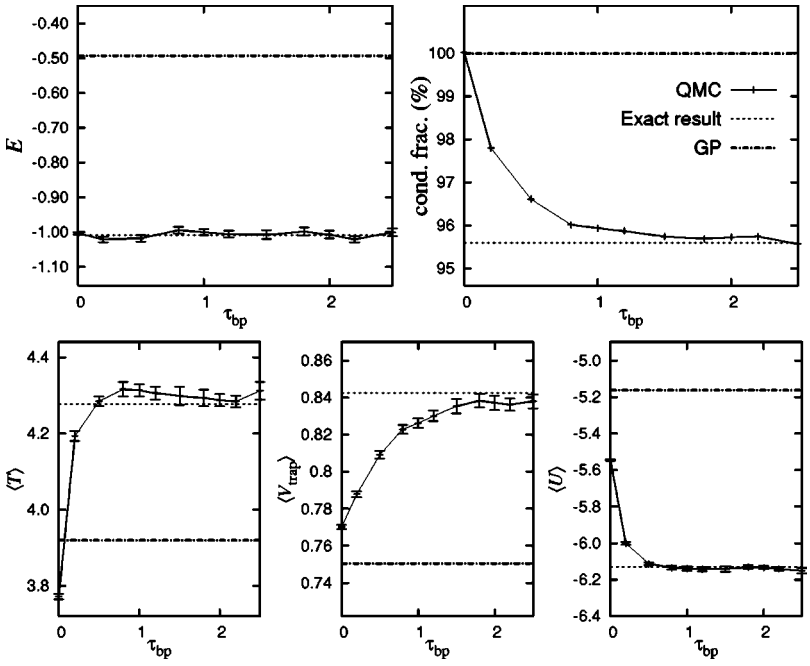

FIG. 2. Convergence of the computed observables versus τ_{bp}. The system is the same as in Table I. The different panels show five different observables. The horizontal axes are the back-propagation length. Exact and GP results are also shown for comparison. Solid lines are present only to aid the eye.

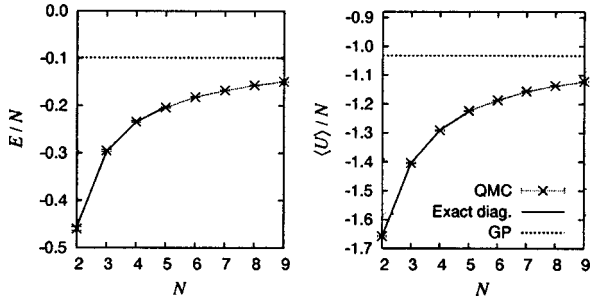

FIG. 4. Comparison of QMC, GP, and ED results for different systems. Calculations were done along a GP isoline $(N-1)U=-2.30t$ for up to nine particles in 13 sites. The graphs show the total and interaction energies *per particle*. QMC and exact results are indistinguishable. GP is accurate in the limit of weak correlation but deviates more from the exact results as the system becomes more correlated.

the effect of correlations. Both the total energy and the interaction energy are lowered from the GP results. The exact results deviate from GP more as the system becomes more correlated, i.e., when U is increased or when N is decreased. Although N is too small here because of the limitation of ED, the results are representative of the general trend in larger systems (see below).

Figure 5 further illustrates the effect of particle correlation in this system. Although the exact interaction energy is lower than that of GP, the exact density profile is more extended. This is also manifested in the average trap potential energy $\langle \hat{V}_{\text{trap}} \rangle / N$, where the QMC results are 0.1981(8) and 0.1605(2) for $N=2$ and 9 particles, respectively, while the GP value is 0.1501. In GP, interaction energy is lowered by increasing particle overlap, namely, by shrinking the profile. In reality, the particles find a way to lower the interaction

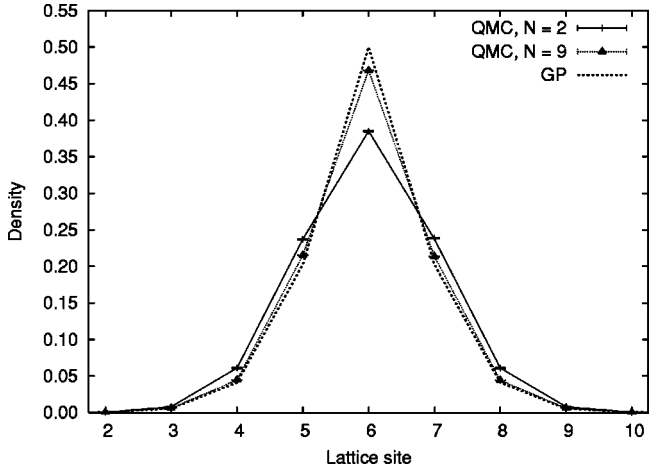

FIG. 5. The normalized density (dimensionless) at different lattice sites. Results are for 13-site systems along the GP isoline $(N-1)U=-2.30t$. The normalized GP curve is identical for any number of particles along this line. QMC results are shown for $N=2$ and $N=9$. The QMC results have very small error bars and are indistinguishable from ED (not shown). The QMC density profiles are more extended, although the interaction energies are lower than GP, as shown in Fig. 4.

TABLE II. Comparison of QMC and GP results to available exact results. The system has 20 particles and $g=0.154$. A lattice of 1024 sites was used, with $\Delta\tau=0.01$ and $\tau_{\text{bp}}=2.5$. For comparison, QMC results without droplet correction (DC) (see Appendix B 2) are also shown.

Type	Ground-state energy	$\langle \hat{T} \rangle$	$\langle \hat{V}_{2B} \rangle$	Cond. frac.
Analytic result	−1.971			
QMC	−1.964(8)	2.044(8)	−4.007(4)	99.76%
QMC (no DC)	−1.851(8)	2.157(8)	−4.007(4)	99.76%
GP	−1.784	1.776	−3.561	100%

energy without statically confining to the central sites, resulting in a more extended one-body profile.

B. Comparison with analytic results in 1D: $a_s<0$

The problem of an arbitrary number of untrapped bosons interacting with an attractive δ potential in one dimension can be solved analytically [34], yielding analytic expressions for the total energy and density profile. In this section, we carry out QMC and GP calculations and compare our results against these analytic results, on systems of up to 400 bosons. The Hamiltonian in the continuous real space is

$$\hat{H} = -\tfrac{1}{2}\sum_{i=1}^{N} \frac{\partial^2}{\partial x_i^2} - \tfrac{1}{2} g \sum_{i>j=1}^{N} \delta(x_i - x_j). \tag{52}$$

The interaction constant $(g>0)$ is related to our Hubbard parameters by $g \equiv |U/\sqrt{t}|$. The ground state of this Hamiltonian is an N-boson bound state. By fixing the center of mass at $x=0$, we can eliminate the contribution from its overall motion, which leads to the following analytic expressions for the density profile [35]:

$$\rho(x) = \tfrac{1}{2} g \sum_{n=1}^{N-1} (-1)^{n+1} \frac{n(N!)^2 e^{-gnN|x|/2}}{(N+n-1)!\,(N-n-1)!}, \tag{53}$$

and the total energy,

$$E = -\tfrac{1}{96} g^2 N(N^2-1). \tag{54}$$

In our QMC calculations, we again put the system on a real-space lattice. The lattice size is chosen to be large enough so that discretization errors are comparable to or smaller than statistical errors. As the ground state of the system is a droplet in the absence of the external confining potential, the center of mass can slide in the calculation due to random noise. We therefore need to subtract the center-of-mass motion, which we will refer to as the *droplet correction*. Technically, this can be accomplished conveniently in the random walk by treating the system with respect to its center of mass. In Appendix B, we describe our method for this correction, which is applicable in any situation where the center of mass and relative motions need to be separated. In our calculations, the correction affects the kinetic and total energies as well as the density profiles. The results shown

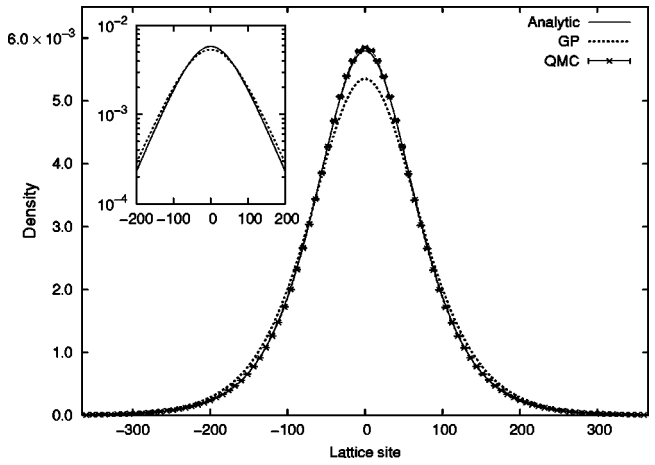

FIG. 6. Comparison of calculated density profiles from QMC and GP with analytical results for the system shown in Table II. The densities are normalized. The QMC error bars are displayed every five data points to avoid cluttering the plot. The inset shows the same curves with logarithmic vertical scale, indicating that at large distances the density is exponential.

below were all obtained with this correction applied.

We first study a system of 20 particles with $g=0.154$. Table II shows the energies, and Fig. 6 the density profiles. This is a system where mean field makes significant errors. Our QMC results are in excellent agreement with the exact results.

We next scan systems with various numbers of particles by following the GP isoline $(N-1)g=4.0$. The energy per particle is shown as a function of N in Fig. 7, for up to 400 particles. Figure 8 shows the density profiles for up to 100 particles. Again, the agreement between QMC and exact results is excellent. As the interaction strength g is increased or as N is decreased, mean-field results deviate more and more from the exact results. For example, as we go from $g=0.01$ ($N=400$) to 10 times the strength along the isoline, the systematic error in the GP total energy increases roughly from 0.5% to 5%.

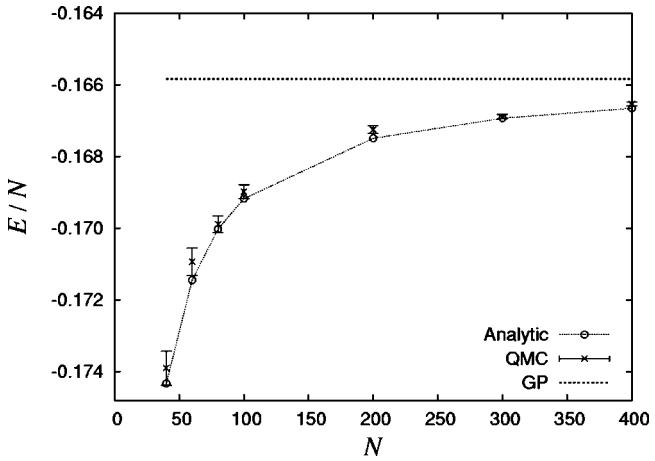

FIG. 7. Comparison of the energy from QMC with the exact answer and GP for a different number of particles. Energy per particle is shown along the GP isoline $(N-1)g=4.0$. We use a lattice of 1024 sites, $\Delta\tau=0.01$, and $\tau_{bp}=4.0$.

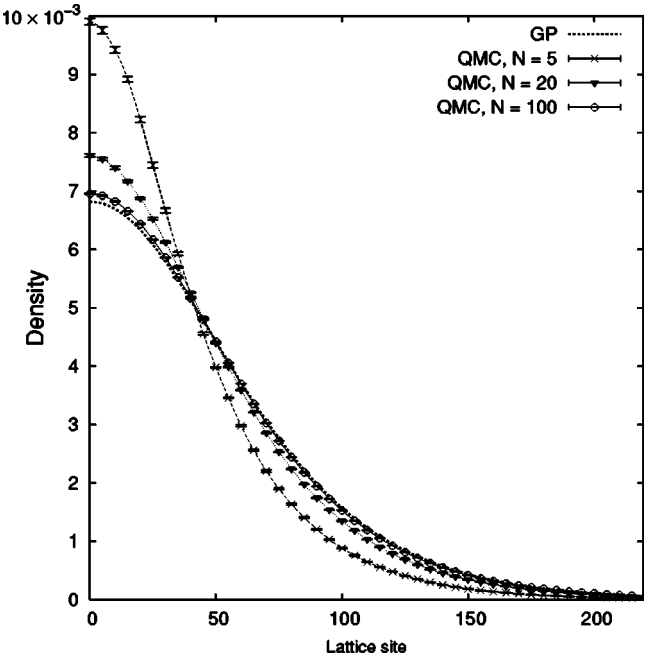

FIG. 8. Comparison of the density profiles from QMC and GP. The normalized densities are shown along the GP isoline $(N-1)g=4.0$ for several N values. The system is the same as that in Fig. 7. The GP density is the same for any N on the isoline.

We now study the system along a different line, holding the interaction strength g fixed while scanning the number of particles, again up to $N=400$ particles. Figure 9 shows the behavior of $\langle\hat{H}\rangle/N^3$, with $g=0.0403$. At large N, the total energy is roughly proportional to N^3. Compared to Figs. 7 and 8, the interaction is stronger at larger N and weaker at lower N, with the crossover at $N\sim100$. Most of the calculations are therefore more challenging numerically. Again QMC was able to completely recover the correlation energy missed by GP. At large N, smaller times steps were used and

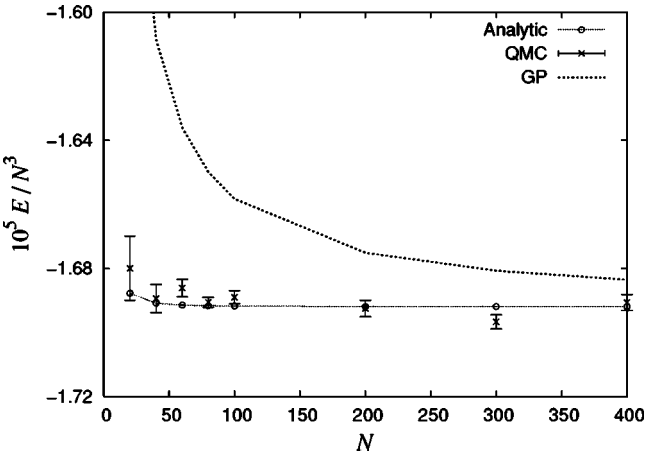

FIG. 9. Comparison of computed ground-state energy for different numbers of particles N. The interaction strength is held constant at $g=-0.0403$. The total energy divided by N^3 is shown as a function of N for QMC, GP, and exact calculations. Conservative QMC parameters were used, with $\tau_{bp}=4.0$ in all case, and $\Delta\tau=0.01$ for $N<200$ and $\Delta\tau=0.005$ otherwise.

TABLE III. Comparison of QMC results against exact diagonalization (ED) and the Gross-Pitaveskii (GP) method in 1D. Here we use 13 sites and 4 particles; $t=2.676, U=+1.538, \kappa=0.3503, \Delta\tau=0.01$, and $\tau_{\mathrm{bp}}=2.5$.

Type	Ground-state energy	$\langle\hat{T}\rangle$	$\langle\hat{V}_{\mathrm{trap}}\rangle$	$\langle\hat{V}_{2B}\rangle$	Cond. frac.
ED	4.24	1.18	1.793	1.269	98.5%
QMC	4.24(2)	1.18(2)	1.790(8)	1.273(8)	98.6%
GP	4.43	1.03	1.800	1.599	100%

more computing was necessary to reduce the statistical errors. (Note that the error bars appear larger at smaller N in the plot because of the division by N^3.)

C. Comparison with exact diagonalization: $a_s>0$

We have shown that our QMC algorithm is exact and works well for a wide range of systems with attractive interactions. If the interaction is repulsive ($a_s>0$, or equivalently $U>0$), the one-body propagators resulting from the HS transformation become *complex*, in the form of $\exp(i\sqrt{\Delta\tau U}x_i\hat{n}_i)$. The same algorithm applies in this case as well. In principle, the complex one-body operator only requires a change to the corresponding complex operations. But in practice a serious phase problem occurs, which causes the calculation to lose efficiency rapidly at larger interaction strengths. We discuss this problem and how to control it below. Our initial studies indicate that, for moderate interaction strengths, the algorithm as is remains very efficient and gives accurate results, allowing reliable calculations for parameters corresponding to experimental situations in 3D.

We benchmark our algorithm in one- and two-dimensional systems with repulsive interactions against exact diagonalization. Table III shows results for a one-dimensional system, with 13 sites and four particles. The agreement between QMC and exact result is excellent. Results from GP are also shown. The GP and QMC density profiles have roughly the same size, as is evident from the values of $\langle\hat{V}_{\mathrm{trap}}\rangle$. However, GP overestimates the interaction energy because it does not take into account the particle-particle correlation. In the mean-field picture, expanding the density profile is the only way to lower the interaction energy, so that the particles overlap less with each other. (Note that $\langle\hat{V}_{\mathrm{trap}}\rangle$ is indeed slightly larger for GP.) In reality, the particles can avoid each other more effectively by means of many-body correlation. The QMC correctly recovers this correlation, which lowers the total energy without spreading the density as much as GP does.

TABLE IV. Comparison of QMC calculations against exact diagonalization (ED) and Gross-Pitaveskii (GP) projection in a 4×4 lattice, with four bosons. $t=0.2534$, $U=+0.3184$, $\kappa=3.700$, $\Delta\tau=0.01$, and $\tau_{\mathrm{bp}}=2.5$.

Type	Ground-state energy	$\langle\hat{T}\rangle$	$\langle\hat{V}_{\mathrm{trap}}\rangle$	$\langle\hat{V}_{2B}\rangle$	Cond. frac.
ED	6.000	1.818	3.8326	0.350	97.8%
QMC	6.005(6)	1.817(2)	3.8325(2)	0.355(5)	97.8%
GP	6.067	1.763	3.8359	0.469	100%

Table IV shows results for bosons in a two-dimensional trap, using a 4×4 lattice. The GP solution also exhibits the same behavior as in the 1D calculation, in that the density profile is slightly more extended, and the interaction energy is overestimated. As in other cases, the QMC statistical error bar on the condensate fraction was not computed directly, but we estimate it to be on the last digit.

As mentioned earlier, the complex propagators cause problems. Since the orbitals and walker weights become complex, asymptotically the phase of these weights will be uniformly distributed in the complex plane. The denominators in Eqs. (34) and (40) will be dominated by noise, causing the Monte Carlo sampling efficiency to decay and ultimately destroying the algebraic scaling of QMC. This is the so-called sign or phase problem [19,21]. In real-space methods, this problem is connected to fermions, but here we have a situation where a phase problem appears in the ground state of a bosonic system. Physically, it is easy to see why a phase problem must occur. Our many-body wave function is being represented in IOR, with only one orbital in each walker. With a repulsive interaction, the only way to reflect correlation effects, i.e., particles avoiding each other, is to make the orbitals complex.

As we see below, our algorithm remains efficient and gives accurate results for large systems with scattering lengths corresponding to experimental situations in 3D. As the interaction strengths become much stronger, the phase problem will ultimately make the approach ineffective. We have done preliminary calculations in which we control the phase problem by applying a phaseless formalism described in Ref. [21]. Our results indicate that the systematic errors introduced by the phaseless approximation are small for moderate interaction strengths. We expect to therefore be able to obtain accurate and reliable results for scattering lengths well into the experimental "strong interaction" regime achievable by Feshbach resonance.

D. Realistic calculations in three dimensions

In this section, we present some test results on realistic systems of trapped particles in three dimensions. QMC results were obtained with back-propagation and conservative choices of $\Delta\tau$ and convergence parameters. We also carry out the corresponding Gross-Pitaevskii calculations, and make comparisons against our exact QMC results. We choose a trap with a characteristic length $a_{\mathrm{ho}}=8546$ Å. The trap was discretized into a $15\times15\times15$ lattice, in a range that corresponds to $5.26a_{\mathrm{ho}}$. Below we will again use reduced units (see Sec. IV A) for the energies. To relate them to realistic physical situations, a multiplicative factor proportional to the inverse atomic mass is needed. For ^{85}Rb atoms, this factor is about 5.7 nK.

Table V shows the result of a QMC calculation for 175 particles in a three-dimensional trap. The scattering length is $a_s=-22.4$ Å. In this regime, the GP solution is a good ap-

TABLE V. Comparisons of QMC and GP calculations for 175 particles in a 3D spherical trap, with $a_s=-22.4$ Å and $a_{\mathrm{ho}}=8546$ Å. The energies are displayed as per-particle quantities. Both the QMC and GP results are extrapolated to $\Delta\tau\to 0$.

Type	Ground-state energy	$\langle\hat{T}\rangle$	$\langle\hat{V}_{\mathrm{trap}}\rangle$	$\langle\hat{V}_{2B}\rangle$	Cond. frac.
QMC	16.979(6)	16.47(5)	6.54(1)	−6.03(4)	99.73%
GP	17.115	15.60	6.77	−5.25	100%

TABLE VI. QMC calculation of 100 particles in a three-dimensional trap. A lattice of $15\times15\times15$ was used. The parameters correspond to $a_{\mathrm{ho}}=8546$ Å and $a_s=80$ Å. The quantities displayed are for per particle.

Type	Ground-state energy	$\langle\hat{T}\rangle$	$\langle\hat{V}_{\mathrm{trap}}\rangle$	$\langle\hat{V}_{2B}\rangle$	Cond. frac.
QMC	24.687(9)	9.573(9)	11.933(5)	3.181(3)	99.80%
GP	24.922	9.281	12.028	3.612	100%

proximation to the exact ground-state wave function. We see that this is indeed the case in Table V. The interaction energy is lowered in the many-body calculation as expected. Interestingly, the external potential energy is lower than in GP. Consistent with this, the exact density profile is tighter than in GP, as shown in Fig. 10. The trend here appears different from what we observed in small 1D trapped systems in Fig. 5, but consistent with the large untrapped systems in Fig. 8. We are presently carrying out more calculations to cover a wider range of parameters and study the role of dimensionality.

We now turn to bosons with repulsive interactions in a three-dimensional trap. We again use a $15\times15\times15$ lattice, and simulate 100 bosons. We choose a scattering length a_s of 80 Å. This value is close to the experimental ^{39}K singlet [36] or ^{87}Rb triplet [37] scattering lengths. In Table VI, we show the calculated energies and condensate fraction. For this interaction strength, the impact of the phase problem on the statistical error is small, and the QMC calculation is very efficient. The true condensate is, like in the 1D repulsive case, tighter than that predicted by GP, with lower interaction energy.

VI. DISCUSSIONS

A. Connection between QMC and Gross-Pitaevskii projections

The QMC method we have presented, which goes beyond mean field and includes many-body correlations, has a deep connection with the GP mean-field approach. Our approach uses an HS transformation which leads to integrals of single-particle operators over auxiliary fields. The mean-field solution can be regarded as the leading term in the stationary-phase asymptotic expansion of the exact solution [38]. Our method evaluates this exact solution, which is in the form of many-dimensional integrals, by Monte Carlo sampling. In this section, we comment further on the formal connection between our importance-sampled QMC and the GP as done by projection (the second of the two GP methods discussed in Sec. IV C).

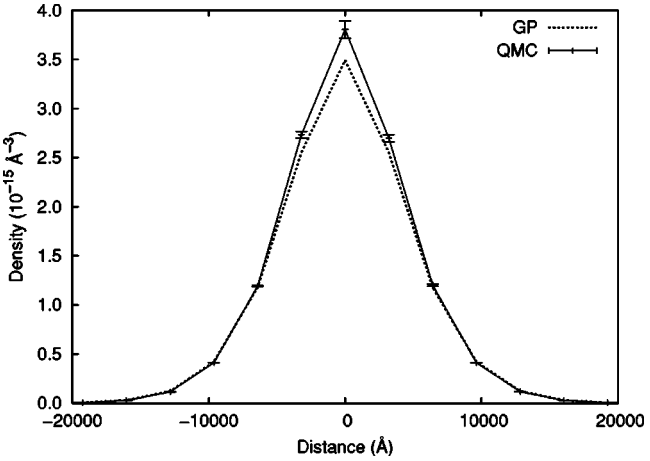

FIG. 10. Comparison of density profiles from the QMC and GP for 175 particles. The system is the same as described in Table V. The QMC profile is more peaked and tighter than GP.

Let us reconsider the two-body propagator in the modified AF transformation, Eq. (25). Let us suppose that we are now taking the first QMC step, where the walker and the trial wave function are both $|\phi\rangle$ $(=|\Psi_T\rangle)$. Following the discussion of the optimal choice of $\vec{x}$ in the same section, Sec. III B, we know that $\vec{x}=0$ is a stationary point with the choice

$$\underline{x}_i=-\sqrt{\Delta\tau}\,\overline{v_i}\equiv-\sqrt{\Delta\tau}\,\frac{\langle\phi|\hat{v}_i|\phi\rangle}{\langle\phi|\phi\rangle}. \tag{55}$$

We can approximate the integral in Eq. (25) by the value of the integrand at $\vec{x}=0$, which can be justified in the limit of small $\Delta\tau$. More explicitly, with a change of the integration variable $\vec{y}\equiv\sqrt{\Delta\tau}\vec{x}$, the integral can be written as

$$e^{(1/2)\Delta\tau\vec{v}^2}=e^{-\Delta\tau[(1/2)\vec{v}^2-\vec{v}\cdot\vec{\hat{v}}]}\int_{-\infty}^{\infty}dy\frac{e^{-y^2/2\Delta\tau}}{\sqrt{2\pi\Delta\tau}}e^{y(\hat{v}-\overline{v})}.$$

As $\Delta\tau\to0$, the dominant contribution to the integral comes from the maximum of the Gaussian at $y=0$. The leading term of the importance-sampled many-body propagator is therefore

$$e^{-\Delta\tau[\hat{K}-\Sigma_i\overline{v}_i\hat{v}_i+(1/2)\Sigma_i\overline{v}_i^2]}, \tag{56}$$

where $\hat{K}$ is the one-body term in the original Hamiltonian. Under this approximation, our random walk becomes deterministic, needing only one walker. If for the next step we use the updated wave function $|\phi'\rangle$ to evaluate the new $\{\overline{v_i}\}$ in Eq. (55), we obtain a self-consistent projection with one-body propagators. In fact, the one-body Hamiltonian in the exponent of Eq. (56) is precisely the mean-field Hamiltonian. For example, for the Bose-Hubbard model the last two terms in the exponent lead to the GP mean-field potential

$$U\sum_i \left(\overline{n_i}\hat{n}_i - \tfrac{1}{2}\overline{n_i^2}\right). \quad (57)$$

Apart from the factor $(N-1)/N$ which approaches unity in the limit of large N, we have recovered the GP propagator. The projection with Eq. (56) lowers the variational energy for any initial $|\phi\rangle$ and is stationary when $|\phi\rangle$ is the GP solution. This is why GP is the best variational wave function that has the form of a single permanent, and hence a reasonable trial wave function to use for most of our QMC calculations.

It is also clear from the discussion above that the importance-sampling formalism allows us to have an optimal form of HS transformation, in that the HS propagator $e^{\nu(\hat{v}-\overline{v})}$ involves only the difference $\hat{v}-\overline{v}$. In other words, although in Eq. (7) we write the decomposition for the bare interaction term, the importance-sampling transformation effectively introduces a mean-field background based on the trial wave function and allows the HS to deal with only a residual quadratic interaction term, $(\hat{v}-\overline{v})^2$.

To summarize, our QMC method reduces to GP if we evaluate the many-body propagator by the stationary-point approximation, using only the centroid of the Gaussian. The full method evaluates the many-dimensional integral over auxiliary fields exactly by Monte Carlo calculation. It captures the interaction and correlation effects with a stochastic, coherent ensemble of mean-field solutions. The structure of the calculation can be viewed as a superposition of the GP projections that we have described. Our method, therefore, provides a way to systematically improve upon GP while using the same framework.

B. Computing

Because of the structure of QMC as a superposition of GP projections, our method scales gracefully with system size. As discussed in Sec. IV B, the bulk of our method scales as $\mathcal{O}(M \log M)$, with the significant speedup from using fast Fourier transform. For example, the QMC calculation shown in Table VI required fewer than 8 h on a single Alpha EV67 processor. The 1024-site QMC calculation shown in Table II took about 4 h to get good statistics, with very conservative choices of $\Delta\tau$ and other convergence parameters. It required about 1.3 gigabytes of memory, largely because of back-propagation path recording. In contrast, treated fully, the latter problem would mean the diagonalization of a sparse, Hermitian matrix containing $(8\times 10^{41})^2$ elements. Although this can be reduced by exploiting symmetries, exact diagonalization of this problem is clearly not within reach with computing capabilities in the foreseeable future.

We typically use hundreds of walkers in our calculation. The stochastic nature of QMC means the number of walkers fluctuates due to branching and killing of walkers with very large and very small weights (see Sec. III). The population therefore must be controlled to ensure that it does not grow or decay too much, and that the walker weights have a reasonable distribution. Our method to control the population is similar to that discussed in Ref. [26].

We comment on the effect of the number of particles, N, on computational scaling. Because of the use of IOR, the algorithm appears as if it only involved a single particle. This is not true, of course, since both the shift $\overline{v_i}$ and the local energy scale with N (see Appendix A). As a result, a smaller time step must be used for larger N. The above argument suggests that $\Delta\tau$ scale *roughly* as $1/N$, which we have used as a guideline in our calculations to select the range of $\Delta\tau$ to use. Extrapolations with separate calculations using different $\Delta\tau$ values are then carried out.

C. Conclusion and outlook

In conclusion, we have presented an auxiliary-field QMC algorithm for obtaining the many-body ground state of bosonic systems. The method, which is based upon the field-theoretical framework and is essentially exact, provides a means to treat interactions more accurately in many-body systems. Our method shares the same framework with the GP approach, but captures interaction and correlation effects with a stochastic ensemble of mean-field solutions. We have illustrated our method in trapped and untrapped boson atomic gases in one, two, and three dimensions, using a real-space grid as a single-particle basis which leads to a Bose-Hubbard model for these systems. We have demonstrated its ability to obtain exact ground-state properties. We have also carried out the GP mean-field calculations and compared the predictions with our exact QMC results. Our method is capable of handling large systems, thus providing the possibility to simulate system sizes relevant to experimental situations. We expect the method to complement GP and other approaches, and become a useful numerical and theoretical tool for studying trapped atomic bosons, especially with the growing ability to tune the interaction strengths experimentally and reach more strongly interacting regimes.

From the methodological point of view, more work remains to be done with the repulsive case to deal with the phase problem. We have shown that our method as it stands can be very useful for moderate interaction strengths. For stronger interactions, our preliminary study indicates that the phaseless approximation [21], which eliminates the phase problem but introduces a systematic error, is very accurate for scattering lengths well into the Feshbach resonance regime. We are currently examining this more systematically to quantify the extent of the bias. Because of the simplicity of these bosonic systems compared to electronic systems, they provide an ideal testbed, where for small sizes the problem is readily solved by exact diagonalization.

A variety of applications are possible. The ground state of the Bose-Einstein condensates with both attractive and repulsive interatomic interactions can be studied for various interaction strengths, including the strongly interacting regime reached by Feshbach resonance. They can also be studied in different dimensions and under different conditions. In particular, it would seem straightforward to generalize our present framework to study rotations and vortices, since we are already dealing with complex propagators and wave functions in the repulsive case. In addition, it will be interesting to treat boson-fermion mixtures with our approach. As mentioned, the auxiliary-field method is already widely used to treat strongly interacting fermion systems.

ACKNOWLEDGMENTS

We thank D. M. Ceperley and H. Krakauer for stimulating discussions. Financial support from NSF (Grant No. DMR-9734041), ONR (Grant No. N00014-97-1-0049), and the Research Corporation is gratefully acknowledged. S.Z. expresses his gratitude to Professor D. M. Ceperley and Professor Richard Martin for their hospitality during a sabbatical visit, where part of the work was carried out. We also thank the Center of Piezoelectric by Design (CPD), where part of our computing was performed.

APPENDIX A: IDENTICAL-ORBITAL REPRESENTATION

In fermion calculations, we must use an $M \times N$ matrix to represent a determinant, because the orbitals must be mutually orthogonal. In the boson case, however, this restriction is absent. The most general form of a many-boson permanent is expensive to compute, having complexity of $\mathcal{O}(NM!)$. But we can choose to make all the orbitals identical. In matrix language, we will have only an M-row column vector. We will term this representation the *identical-orbital representation* (IOR). Each many-boson wave function in IOR has the form of a GP mean-field solution. Two conditions are necessary for this choice to be viable in the QMC, namely that an initial trial wave function of this form is allowed and that successive projections preserve the form. The only requirement for the former to hold is that the wave function in IOR not be orthogonal to the true many-body ground state, and it is straightforward to show that Eq. (12) holds for a $|\phi\rangle$ in this form. More complex wave functions can always be generated by a linear combination of such wave functions. In fact, this is what we accomplish through our Monte Carlo simulation.

In operator language, a single N-boson wave function $|\phi\rangle$ is given by

$$|\phi\rangle = \underbrace{\hat{\phi}^\dagger \hat{\phi}^\dagger \cdots \hat{\phi}^\dagger}_{N} |0\rangle = (\hat{\phi}^\dagger)^N |0\rangle,$$

where $\hat{\phi}^\dagger \equiv \Sigma_\alpha c_\alpha^\dagger \phi_\alpha$. In matrix form, $|\phi\rangle$ would be $M \times N$ matrix $\boldsymbol{\phi}$ whose columns are identical. The overlap of two such wave functions is given by

$$\langle \psi | \phi \rangle = \mathrm{per}(\boldsymbol{\psi}^{\mathrm{T}} \cdot \boldsymbol{\phi}) = N!\,(\boldsymbol{\psi}^\dagger \cdot \boldsymbol{\phi})^N,$$

where the boldface symbols $\boldsymbol{\psi}$ and $\boldsymbol{\phi}$ represent the single-column vectors for ψ and ϕ, respectively. Similarly, for any one-body operator $\hat{A}$,

$$\langle \psi | \hat{A} | \phi \rangle = N!\; N(\boldsymbol{\psi}^\dagger \cdot \mathbf{A} \cdot \boldsymbol{\phi})(\boldsymbol{\psi}^\dagger \cdot \boldsymbol{\phi})^{N-1}, \tag{A1}$$

where $\mathbf{A}$ is the matrix for $\hat{A}$. The matrix element of a quartic (two-body) operator is given by

$$\langle \psi | b_\alpha^\dagger b_\beta^\dagger b_\gamma b_\delta | \phi \rangle = N!\; N(N-1)\psi_\alpha^* \psi_\beta^* \phi_\gamma \phi_\delta (\boldsymbol{\psi}^\dagger \cdot \boldsymbol{\phi})^{N-2}. \tag{A2}$$

APPENDIX B: DROPLET CORRECTION

1. Correcting the density broadening

To handle the droplet system given by the translationally invariant Hamiltonian in Eq. (52), an extra ingredient is necessary in addition to the "basic" QMC algorithm that we have described. In a deterministic calculation, for example in GP, the motion of the center of mass (c.m.) can be simply eliminated by fixing it at the origin, as in Eq. (53). In the QMC calculation, however, the orbitals fluctuate as they are propagated by $\hat{B}(\vec{x}-\vec{x})$, where the random fields $\vec{x}$ are drawn from a Gaussian probability density. Random noise will inevitably cause the c.m. of the system to slide, undergoing a free diffusion whose average position is the origin.

Left unchecked, this spurious c.m. motion will lead to an artificial broadening of the density profile. To correct for it in the density profile, we could simply shift the c.m. of every walker back to the origin. However, the importance-sampled propagator involves ratios of overlaps with the trial wave function $\langle \Psi_T | \phi_i \rangle$, which would have to be corrected in the random walk whenever a shift is made.

Our solution is to let the trial wave function slide along with the walkers. In other words, we rewrite the kinetic energy operator as

$$\hat{T} = \hat{T}_{\mathrm{c.m.}} + \hat{T}', \tag{B1}$$

where $\hat{T}_{\mathrm{c.m.}}$ represents the c.m. kinetic energy and $\hat{T}'$ the internal kinetic energy *in* the c.m. frame. The total Hamiltonian is given by

$$\hat{H} = \hat{T}_{\mathrm{c.m.}} + \hat{T}' + \hat{V} \equiv \hat{T}_{\mathrm{c.m.}} + \hat{H}'. \tag{B2}$$

The quantities that we wish to compute are governed by the "internal" Hamiltonian $\hat{H}'$. Since $\hat{V}$ involves only relative coordinates among the particles, it commutes with $\hat{T}_{\mathrm{c.m.}}$; or more generally,

$$[\hat{T}_{\mathrm{c.m.}}, \hat{H}'] = 0. \tag{B3}$$

In this way, the importance-sampled QMC propagation is determined by $\hat{H}'$. The motion of the c.m. in each walker is a separate free diffusion which is governed by $\hat{T}_{\mathrm{c.m.}}$. In the random-walk process, we are now free to correct for the c.m. motion by shifting the walkers back to the origin whenever necessary. For consistency, this correction must be applied both in the normal random walk and in the back-propagation phase.

2. Separating the center-of-mass kinetic energy

The moving trial wave function, however, poses a problem for the calculation of the kinetic energy. Now the orbitals are free to slide, and the diffusive motion of the orbital's c.m. is no longer suppressed in the laboratory frame. When we use the usual t term in the Hamiltonian in Eq. (43) to compute the kinetic energy, we obtain the total $\langle \hat{T} \rangle$, in which $T_{\mathrm{c.m.}} \equiv \langle \hat{T}_{\mathrm{c.m.}} \rangle$ and the desired $\langle \hat{T}' \rangle$ are mixed. This leads to a spurious increase in the estimate of the kinetic energy and

consequently the total energy, as shown in Table II. Since we know the nature of the c.m. motion, it is fairly straightforward to extract $T_{\text{c.m.}}$ and explicitly subtract it from the kinetic and total energy estimates. Allowing the droplet to freely slide in the calculation is equivalent to having a spurious "propagator" $e^{-\Delta\tau\hat{T}_{\text{c.m.}}}$, whose effect on the wave function for the c.m. is described by the diffusion equation

$$-\frac{\partial\Psi_{\text{c.m.}}(\mathbf{R},\tau)}{\partial\tau}=\hat{T}_{\text{c.m.}}\Psi_{\text{c.m.}}(\mathbf{R},\tau).$$

It is a well known property of such a diffusion process that the averaged squared distance $\langle\mathbf{R}^2(\tau)\rangle$ grows linearly with the (imaginary) time τ,

$$\langle\mathbf{R}^2(\tau)\rangle=b\tau.$$

We can obtain b by recording the quantity $\langle\mathbf{R}^2(\tau)\rangle$ for a period of time in the QMC simulation. The constant b is linearly proportional to $T_{\text{c.m.}}$. More specifically, the c.m. Hubbard hopping parameter $t_{\text{c.m.}}$ can be extracted from b,

$$t_{\text{c.m.}}=b/2. \tag{B4}$$

This gives us the correct kinetic and total energies,

$$\langle\hat{T}'\rangle=\left(1-\frac{t_{\text{c.m.}}}{t}\right)\langle\hat{T}\rangle, \tag{B5a}$$

$$\langle\hat{H}'\rangle=\langle\hat{T}'\rangle+\langle\hat{V}_{2B}\rangle. \tag{B5b}$$

To conclude, there are two necessary modifications in the QMC algorithm in order to treat quantum droplets.

(i) We let the trial wave function effectively "follow" the QMC orbitals, by defining its c.m. according to that of each QMC orbital.

(ii) For each orbital, we accumulate all the applied c.m. shifts in order to estimate $\langle\mathbf{R}^2(\tau)\rangle$. This gives us the fraction of c.m. kinetic energy through the constant $t_{\text{c.m.}}$.

[1] M. H. Anderson, J. R. Ensher, M. R. Matthews, C. E. Wieman, and E. A. Cornell, Science **269**, 198 (1995).
[2] F. Dalfovo, S. Giorgini, L. P. Pitaevskii, and S. Stringari, Rev. Mod. Phys. **71**, 463 (1999).
[3] A. J. Leggett, Rev. Mod. Phys. **73**, 307 (2001).
[4] S. L. Cornish, N. R. Claussen, J. L. Roberts, E. A. Cornell, and C. E. Wieman, Phys. Rev. Lett. **85**, 1795 (2000).
[5] W. M. C. Foulkes, L. Mitas, R. J. Needs, and G. Rajagopal, Rev. Mod. Phys. **73**, 33 (2001), also see the references therein.
[6] D. M. Ceperley, Rev. Mod. Phys. **67**, 279 (1995), and also the references therein.
[7] W. Krauth, Phys. Rev. Lett. **77**, 3695 (1996).
[8] P. Grüter, D. Ceperley, and F. Laloë, Phys. Rev. Lett. **79**, 3549 (1997).
[9] M. Holzmann and W. Krauth, Phys. Rev. Lett. **83**, 2687 (1999).
[10] J. L. DuBois and H. R. Glyde, Phys. Rev. A **63**, 023602 (2001).
[11] J. L. DuBois and H. R. Glyde, Phys. Rev. A **68**, 033602 (2003).
[12] M. Ulmke and R. T. Scalettar, Phys. Rev. B **61**, 9607 (2000).
[13] R. Blankenbecler, D. J. Scalapino, and R. L. Sugar, Phys. Rev. D **24**, 2278 (1981).
[14] G. Sugiyama and S. E. Koonin, Ann. Phys. (N.Y.) **168**, 1 (1986).
[15] J. Hubbard, Phys. Rev. Lett. **3**, 77 (1959).
[16] R. D. Stratonovich, Dokl. Akad. Nauk SSSR **115**, 1907 (1957).
[17] J. E. Hirsch, Phys. Rev. B **28**, 4059 (1983).
[18] S. R. White, D. J. Scalapino, R. L. Sugar, E. Y. Loh, J. E. Gubernatis, and R. T. Scalettar, Phys. Rev. B **40**, 506 (1989).
[19] S. Zhang, J. Carlson, and J. E. Gubernatis, Phys. Rev. B **55**, 7464 (1997).
[20] S. Zhang, Phys. Rev. Lett. **83**, 2777 (1999).
[21] S. Zhang and H. Krakauer, Phys. Rev. Lett. **90**, 136401 (2003).
[22] D. J. Dean and S. E. Koonin, Phys. Rev. C **60**, 054306 (1999).
[23] S. Fantoni, A. Sarsa, and K. E. Schmidt, Phys. Rev. Lett. **87**, 181101 (2001).
[24] H. F. Trotter, Proc. Am. Math. Soc. **10**, 545 (1959).
[25] M. Suzuki, Commun. Math. Phys. **51**, 183 (1976).
[26] S. Zhang, in *Theoretical Methods for Strongly Correlated Electrons*, edited by D. Sénéchal, A.-M. Tremblay, and C. Bourbonnais, CRM Series in Mathematical Physics (Springer, New York, 2003), pp. 39–74.
[27] D. R. Hamann and S. B. Fahy, Phys. Rev. B **41**, 11352 (1990).
[28] J. W. Moskowitz, K. E. Schmidt, M. A. Lee, and M. H. Kalos, J. Chem. Phys. **77**, 349 (1982).
[29] P. J. Reynolds, D. M. Ceperley, B. J. Alder, and W. A. Lester, J. Chem. Phys. **77**, 5593 (1982).
[30] E. P. Gross, Nuovo Cimento **20**, 454 (1961).
[31] E. P. Gross, J. Math. Phys. **4**, 195 (1963).
[32] L. P. Pitaevskii, Sov. Phys. JETP **13**, 451 (1961).
[33] P. A. Ruprecht, M. J. Holland, K. Burnett, and M. Edwards, Phys. Rev. A **51**, 4704 (1995).
[34] J. B. McGuire, J. Math. Phys. **5**, 622 (1964).
[35] F. Calogero and A. Degasperis, Phys. Rev. A **11**, 265 (1975), see also the references therein.
[36] J. L. Bohn, J. P. Burke, C. H. Greene, H. Wang, P. L. Gould, and W. C. Stwalley, Phys. Rev. A **59**, 3660 (1999).
[37] J. Weiner, V. S. Bagnato, S. Zilio, and P. S. Julienne, Rev. Mod. Phys. **71**, 1 (1999).
[38] J. W. Negele and H. Orland, *Quantum Many-Particle Systems*, Advanced Book Classics (Perseus, Reading, MA, 1998).